UPPSALA
UNIVERSITET

Digital Comprehensive Summaries of Uppsala Dissertations from the Faculty of Science and Technology 1216

Wireless Interface Technologies for Sensor Networks

MAGNUS JOBS

ACTA
UNIVERSITATIS
UPSALIENSIS
UPPSALA
2015

ISSN 1651-6214
ISBN 978-91-554-9136-9
urn:nbn:se:uu:diva-239400

Dissertation presented at Uppsala University to be publicly examined in Ångströmslaboratoriet, Lägerhyddsvägen 1, Uppsala, Friday, 13 February 2015 at 13:15 for the degree of Doctor of Philosophy. The examination will be conducted in English. Faculty examiner: doc. Andrei Sazonov (Scanreco Industrielektronik AB).

Abstract

Jobs, M. 2015. Wireless Interface Technologies for Sensor Networks. *Digital Comprehensive Summaries of Uppsala Dissertations from the Faculty of Science and Technology* 1216. 97 pp. uppsala: Acta Universitatis Upsaliensis. ISBN 978-91-554-9136-9.

The main focus of the work presented in this thesis concerns the development and improvement of Wireless Sensor Networks (WSNs) as well as Wireless Body Area Networks (WBANs). WSN consist of interlinked, wireless devices (nodes) capable of relaying data wirelessly between the nodes. The applications of WSNs are very broad and cover both wireless fitness monitoring systems such as pulse watches or wireless temperature monitoring of buildings, among others.

The topics investigated in the work presented within this thesis covers antenna design, wireless propagation environment evaluation and modeling, adaptive antenna control and wireless nodes system design and evaluation. In order to provide an end-user suitable solution for wireless nodes the devices require both small form factor and good performance in order to be competitive on the marked and thus the main part of this thesis focuses on techniques developed and data collected to help achieve these goals.

Several different prototype systems have been developed which have been used to measure data by the Swedish Defence Research Agency (FOI), GKN Aerospace Sweden AB, the Swedish Transport Administration. The system developed with GKN Aerospace was used to do real-time test measurements inside a running RM12 jet engine and required a substantial amount of measurements, environmental modeling and system validation in order to properly design a wireless system suitable for the harsh and fast fading environment inside a jet engine. For FOI improvements were made on a wearable wireless body area network initially developed during the authors master thesis work. Refinements included work on new generation wireless nodes, antenna packaging and node-supported diversity techniques.

Work and papers regarding the design of different types of antennas suitable for wireless nodes are presented. The primary constraints on the presented antennas are the limited electrical size. The types of antennas developed include electrically small helix antennas manufactured both on stretchable substrates consisting of a PDMS substrate with Galinstan as the liquid metal conductors, screen printed silver ink for helix antennas and conformal dual patch antennas for wireless sensor nodes. Other standard type antennas are included on the wireless sensors as well.

Keywords: Wireless Sensor Networks, Body Area Networks, Jet Turbine, Electrically Small Antennas, Antenna Theory, WISENET, Wisejet

Magnus Jobs, Department of Engineering Sciences, Solid State Electronics, Box 534, Uppsala University, SE-75121 Uppsala, Sweden.

ISSN 1651-6214
ISBN 978-91-554-9136-9
urn:nbn:se:uu:diva-239400 (http://urn.kb.se/resolve?urn=urn:nbn:se:uu:diva-239400)

Dedicated to Leksand

List of Papers

This thesis is based on the following papers, which are referred to in the text by their Roman numerals.

I **Magnus Jobs,** Klas Hjort, Anders Rydberg, Zhigang Wu, "A Tunable Spherical Cap Microfluidic Electrically Small Antenna" *Small*, 2013 9(19):3230–3234

II **Magnus Jobs**, Mathias Grudén, Paul Hallbjörner, Anders Rydberg, "Antenna Diversity With Opportunistic Combining for ASK Systems With Single Channel Receivers". Presented at Conference on Antennas and Propagation (*EuCAP*) 2010, Barcelona.

III Mathias Grudén, **Magnus Jobs,** Anders Rydberg "Empirical Tests of Wireless Sensor Network in Jet Engine Including Characterization of Radio Wave Propagation and Fading" Antennas and Wireless Propagation Letters, IEEE, 2014 13:762-765

IV **Magnus Jobs,** Mathias Gruden, Anders Rydberg "Modeling of EM Propagation in Simplified Jet Turbine Structure using Helical Rays ", submitted to IET Electronic Letters, Dec 2014

V Zhigang Wu, **Magnus Jobs**, Klas Hjort, Anders Rydberg " Hemispherical Coil Electrically Small Antenna Made by Stretchable Conductors Printing and Plastic Thermoforming" Accepted for publication in Journal of Micromechanics and Microengineering

VI Mathias Grudén, **Magnus Jobs** and Anders Rydberg "Measurements and Simulations of Wave Propagation for Wireless Sensor Networks in Jet Engine Turbines", *Antennas and Wireless Propagation Letters*, IEEE, *2011* 10:1139 – 1142

VII **Magnus Jobs**, Anders Rydberg "Conformal dual patch antenna for diversity based sensor nodes" *Electronics Letters*, 2012, 48(6): 306 – 307

VIII **Magnus Jobs,** Mathias Grudén, Anders Rydberg, "Performance Evaluation of Conformal Dual Patch Antenna In Indoor Environment", Conference on Antennas and Propagation (*EuCAP*) 2013, Gothenburg.

IX Mathias Grudén, **Magnus Jobs**, "Diversity Techniques for Robustness and Power Awareness in Wireless Sensor Systems for Railroad Transport Applications", book chapter in "*Sustainable Wireless sensor networks*", 2010 , ISBN 978-953-307-297-5

X **Magnus Jobs**, J. Bestoon, F. Lantz, B. Lewin, E. Jansson, J Antoni, K. Brunberg, P. Hallbjörner, A. Rydberg. "Wireless Body Area Network (WBAN) Monitoring Application System(MASS) for Personal Monitoring" *pHealth* conference June 2009, Oslo Norway

Comments on the author's main contribution to the papers

I Antenna design, antenna simulation and modeling, manufacturing of antenna holder, antenna measurements.

II Idea was developed in cooperation between all three authors and the paper was written in cooperation. Device under test built by me.

III The system was designed and tested in cooperation between all authors. The planning of wave propagation measurements and final tests, performing the measurements and writing the manuscript were in cooperation with the first author, Mathias Grudén.

IV Basic concept was develop in shared cooperation between all authors. Further model development, simulations, measurement setup and measurements were performed by me.

V Antenna design, antenna simulations, measurements and antenna holder was done by me.

VI The planning of wave propagation measurements, performing the measurements and writing the manuscript were in cooperation with the first author, Mathias Grudén.

VII Antenna design, manufacturing, simulation and measurements performed by me.

VIII Measurement planning, measurement setup and measurements primarily done by me.

IX Book chapter was written as an cooperation between Mathias Grudén and me. Described and tested circuit built by me and design in cooperation.

X The work presented is a continuation of the work done in original master thesis. The development of sensor hardware and inverse kinematic algorithms were done by me. System tests were performed in cooperation between all authors.

Related Papers

The following papers including the author is not included in the thesis due to being covered in other papers or out of the scope of the thesis

XI Anders Rydberg, Mathias Grudén and **Magnus Jobs**, "Wave Propagation in Jet Engine Turbines", Antenna EMB, Stockholm 2012.

XII **Magnus Jobs,** Mathias Grudén, Anders Rydberg, Sanel Zenkic, Edvard Svenman, Melker Härefors, Olof Hannius, Are Björneklett, Peter Nilsson and Jakob Viketoft. "Wireless Sensor Networks for Aircraft Engines", *Smart Systems Integration* conference March 2011, Dresden Germany.

XIII Magnus Karlsson, Owais Owais, Joakim Öst, Adriana Serban, Shaofang Gong, **Magnus Jobs**, Mathias Grudén " Dipole Antenna With Integrated Balun For Ultra-Wideband Radio 6-9 GHz",Microwave and Optical Technology Letters, Vol. 53, No. 1 January 2011

XIV Jeong SH, Hagman A, Hjort K**, Jobs M**, Sundqvist J, Wu Z. "Liquid alloy printing of microfluidic stretchable electronics", Lab Chip. 2012 Oct 16;12(22):4657-64

XV Anders Rydberg, Mathias Grudén, **Magnus Jobs,** "Wireless Sensors Networks in Electromagnetically and Physically Hostile Environments", Smart Systems Integration, Amsterdam 2013.

XVI Owais Owais, Magnus Karlsson, Shaofang Gong, Zhinong Ying, Mathias Grudén and **Magnus Jobs**, "Wideband planar antenna with modified ground plane" Microwave and Optical Technology Letters, Vol.: 52, Issue: 11, Page(s): 2581-2585, 2010.

XVII Jouni Rantakokko, Joakim Rydell, Peter Strömbäck, Peter Händel, Jonas Callmer, David Törnqvist, Fredrik Gustafsson, **Magnus Jobs**, Mathias Grudén, "Accurate and Reliable Solder And First Responder Indoor Positioning: Multisensor Systems and Cooperative Localization",IEEE Wireless Communications, April 2011

XVIII **Magnus Jobs** "Wireless Diversity and Robustness in WBAN nodes" European Microwave Week 2012, Workshop 01: Wireless Sensors and Sensor Systems in emerging hostile applications, EuMW2012

XIX **Magnus Jobs**, Mathias Grudén, Anders Rydberg "Wireless body area networks (WBANs) and efficient energy conservative designs" GigaHertz Symposium 2010, Lund

XX Jaff Bestoon, **Magnus Jobs**, et al "A Wireless Body Area Network (WBAN) based Tracking and Monitoring Application System" The IET Conference on Body-centric wireless communications, Savoy Place, London, UK. 20 April 2009

XXI Mathias Grudén, **Magnus Jobs** and Anders Rydberg, "Design and Evaluation of a Conformal Patch Antenna Array for use with Wireless Sensor Network inside Jet Engines", Antennas and Propagation (EuCAP), Proceedings of the 7th European Conference on, Gothenburg, 2013.

XXII Paul Hallbjörner, Mathias Grudén and **Magnus Jobs** "Broadband Space-Time Measurements in Reverberation Chamber Including Comparison With Real Environment", Antennas and Wireless Propagation Letters, IEEE, Vol.: 8, Page(s): 1111-1114, 2009.

Contents

Abbreviations

AUT	Antenna Under Test
ASK	Amplitude Shift Keying
BAN	Body Area Network
BW	Bandwidth
c	Speed of light in vacuum
C	Capacitance
CNC	Computer Numerical Control
dB	Decibel measure relative to 1 W
dBm	Decibel measure relative to 1 mW
DUT	Device Under Test
ESA	Electrically Small Antenna
f	Frequency
FET	Field Effect Transistor
FSK	Frequency Shift Keying
GSG	Ground Signal Ground
I	Current
IC	Integrated Circuit
k	Wavenumber
L	Inductance
LAN	Local Area Network
Mbps	Megabit per second
MEMS	Microelectromechanical System
PA	Power Amplifier
PAN	Personal Area Network
PCB	Printed Circuit Board
PNA	General Purpose Network Analyzer
PSTD	Phase Sweep Transmit Diversity
RF	Radio Frequency
RL	Loss Resistance
RLC	Resistance Inductance Capacitance
RR	Radiation Resistance
S_{ij}	S-Parameter between i and j
S_{11}, S_{22}	Reflection Coefficient
S_{12}, S_{21}	Transmission Coefficient
SMD	Surface Mount Device
uC	Microcontroller

VNA	Vector Network Analyzer
WBAN	Wireless Body Area Network
WISENET	Wireless Vinn Excellence Center for Wireless Sensor Networks
WISEJET	Wireless Sensor Network for Jet Engines
WLAN	Wireless Local Area Network
WPAN	Wireless Personal Area Network
W_m	Average magnetic energy
W_e	Average electric energy
WSN	Wireless Sensor Network
X	Reactance
XC	Reactance of capacitor
XL	Reactance of inductor
Z	Impedance
Z_{ij}	Mutual Impedance between i and j
Z_{id}	Drive impedance of port i
λ	Wavelength
ε_0	Permittivity of freespace
ε_r	Relative permittivity
η	Efficiency
η_{rad}	Radiation Efficiency
ω	Angular frequency
μ_0	Permeability of freespace
μ_r	Relative permeability
ρ_c	Correlation coefficient
ρ	Resistivity
σ	Conductivity
φ	Phase

1. Introduction

If a number of small, self-sustained devices could be placed in an area with the ability to transmit data and measurements on the environment (temperature, movement, rainfall etc.) what could this data be used for and how do we design and manufacture such devices?

The question posed above is an attempt to simplify what the area of wireless sensor networks (WSNs) is all about. The idea of being able to remotely access valuable data about an environment or an item situated in a remote environment. It should be noted firstly that such a concept is not new in the sense that researchers and sci-fi writes has touched upon the subject for a long time, however, it is only in the recent decades that the technology required to actually manufacture such devices has advanced far enough.

One of the primary ignitions for the boom in the research of wireless sensor networks came from the Smart Dust project selected for funding by DARPA in 1998. The proposal, presented by K. Pister et. al. [1], embraced the idea and advantages of distributing numerous wireless devices in a selected area in order to help achieve military superiority. From that moment on the research in wireless sensor networks has boomed. It is also worth mentioning that the initial devices presented in the DARPA proposal used optical rather than microwave or RF as a means of communication.

During the years between 2005-2015 wireless devices started appearing on the market and it is today a fairly common technology. In today's market wireless sensors can take the form of health braces used to track one's training regime, wireless LEDs to control the lighting conditions in one's house, wireless GPS monitors to track hunting dogs or to simply remotely keep track of a buildings temperature conditions. The applications are numerous and still growing.

The research field of wireless sensor networks is still relatively young and a great amount of work remains before we can fully reap all the benefits that such a technology brings to the table. It is the purpose of this thesis to present the work done by the author on developing and testing new WSN systems as well as presenting specific new technologies developed to help improve the overall performance of wireless sensor devices.

1.1 Wireless Sensor Networks

The main work on wireless sensor networks presented in this thesis covers two wireless networks with different topics. The first part of the thesis outlines a brief overview of general wireless sensor networks, with additional focus on specific types of wireless sensor networks designed and tested as part of the work presented in the thesis.

The current (at the time of writing this thesis) state of wireless sensor networks is presented in Figure 1.1. Figure 1.1. shows the Gartner Hype Cycle with the current state of a selected few sub-genres of wireless sensor networks marked. The data is based on Gartner's 2014 analysis [2]. The state of Machine to Machine Communications and Mobile Health Monitoring, two areas covered by this thesis, are considered to have passed the hype peak and starting to reach a more mature state.

In the authors view this is a good thing, although funding for research on wireless sensor networks can be considered more difficult to obtain as the hype curve has been passed, the advantages of a more fundamental theoretical base as well as more mature technologies could be considered to give much more robust and well developed base on which to develop further technologies. It is also worth mentioning that in the initial stages of the work presented in this thesis the area of WSNs stood right at the peak of the hype curve and the author has had the privilege to both be a part of a field covered with dreams and expectations as well as a more mature technological scene.

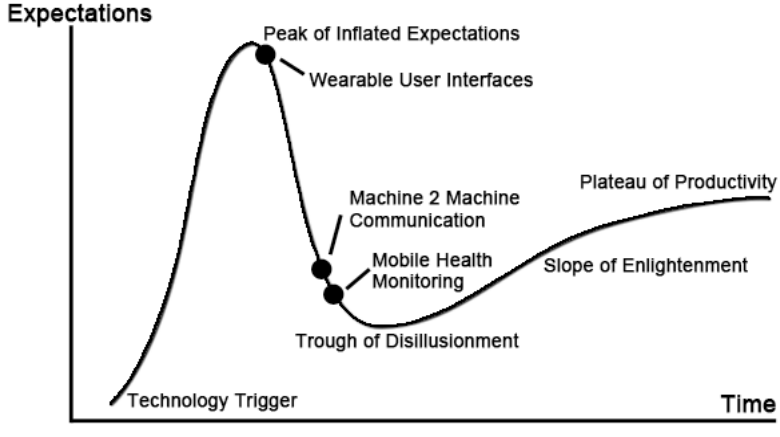

Figure 1.1. Hype curve showing state of wireless networks as of 2014

1.1.1 Wireless Body Area Networks

The wireless network presented in the first section of the thesis was developed for the Swedish Defense Research Agency (FOI) within the WISENET project with the intention to provide real time monitoring of soldier movement and kinematics. WISENET was a joint project funded by VINNOVA and is an abbreviation for Uppsala VINN Excellence Center for Wireless Sensor Networks. WISENET was a cooperation between Uppsala University, Swedish Administrations and Institutes as well as commercial companies. The system was developed and field tested by the FOI and presented in a individual report [3].

1.1.2 Wireless Networks in Jet Turbines

The second network presented is a wireless sensor network for engine monitoring of jet turbines. The project was a cooperation between Uppsala University, ÅAC Microtec AB and GKN Aerospace Engine Systems, Sweden (formerly Volvo Aero) as the work leader. The main purpose of the system was to monitor engine parameters in the fan stage of a running jet turbine. Due to a substantial amount of nearby metal components, rotating parts and high temperatures the environment provides a highly challenging harsh environment for the network to operate in.

This thesis also presents data on the design, modeling and testing of the wireless sensor system. In order to maximize the performance of the sensor network a large amount of work on pre-installation measurements and simulations were required in order to make sure that the system would perform adequately during the final test phase in a running jet turbine.

1.2 Diversity combining for Wireless Sensor Networks

As part of the work presented on wireless sensor networks some additional work was performed on the development of diversity combing schemes for wireless sensor nodes. Since many wireless sensors are placed in electromagnetically "less than ideal" environments significant variations in signal strengths can substantially reduce the overall performance of the network. If a node can be fitted with two or more antennas which exhibits low correlation the sensitivity to fast variations in signal strengths can be reduced and overall performance improved. This thesis focuses mainly on how phase sweep diversity could potentially be used to improved node performance without excessive increases in system complexity.

1.3 Antenna Design for Wireless Networks

Proper antenna design is crucial to any wireless network. If the node's embedded electronics and firmware are the heart and soul of a wireless network the antenna and communication channel are the veins. The work presented in this thesis mainly focuses on electrically small antennas suitable for wireless nodes. Section 6 presents some general outlines for wireless node antenna design important for the following work presented in the thesis.

1.3.1 Hemispherical Coil Antennas

Hemispherical coil antennas are adaptations of the old and well known concept of spherical coil antennas presented by Wheeler [4]. The main difference between the concepts described by Wheeler and more modern adaptations is mainly the usage of hemispherical designs with a ground plane. These types of design can be very useful for wireless nodes as they combine a very good size/efficiency tradeoff and allows for mounting on conducting media. The thesis presents two iterations of hemispherical antennas designs useful for wireless sensor networks.

1.3.2 Conformal Antennas

The primary challenge for any wireless node design is size constrains and keeping the performance high while reducing overall node volume. Since any passive antenna is bound to very real physical laws limiting the performance on smaller scales it is important to always make use of the highest possible antenna volume for designs. One example of such a solution is by using the outer surface of a nodes packaging for antenna placement. This form of conformal antenna design, in the sense that the antenna conforms to the surface of the node package, is of high interest for wireless sensors. In this thesis one example is presented which used a pair of conformably mounted, low correlation patch antennas in order to allow for the implementation of diversity schemes on the node side.

1.4 Thesis Outline

The work presented in the thesis is arranged in such a way that it starts with information about the two major types of wireless networks designed and tested as part of the work presented. Once the two different networks has been presented the thesis goes a bit into detail on the sub-packages of work carried out on specific key-components of the wireless sensor networks. This primarily covers a brief electrically small antenna primer, diversity schemes, modeling of the turbine environment and antenna design. The different topics and papers presented in the thesis is outlined following:

Chapter 2 covers a general overview of wireless sensor networks and works as a primer for the subsequent chapters on more specific network applications.

Chapter 3 describes a designed body area network for soldier monitoring and the various subcomponents.

Chapter 4 describes a wireless sensor network designed and mounted in the fan stage of a running military grade jet turbine, providing continuous performance data during test-runs.

Chapter 5 describes the advantages and methodology of using diversity combining in wireless nodes. A specific example based on work related to phase sweep diversity combining for wireless sensor nodes is presented.

Chapter 6 gives an overview of different design parameters for wireless node antennas. The purpose is to act as a short primer for the specific antenna designs presented in the following chapters.

Chapter 7 describes how hemispherical coil antennas can be used to provide antennas with good tradeoff between electrical size and efficiency, useful for wireless sensor nodes.

Chapter 8 describes how conformal patch antennas can be used to provide a multi antenna system for a wireless node and some performance measurements to provide example data of how multiple antennas can improve the performance of wireless nodes.

2. Wireless Sensor Networks

Wireless Sensor Networks (WSNs) are a number of either general or special purpose devices (or nodes) which gathers data and relays this wirelessly to other nodes in the network. This data is than either stored and/or acted upon by the network. Wireless sensor networks and especially wireless devices is the main focus of a large amount of the presented work. It therefore serves the purpose to provide a general, albeit brief, overview of wireless networks, devices and the typical characteristics and considerations that should be done when designing a wireless sensor. The intention of this is to serve as a primer for some of the design tradeoffs which are presented in the following chapters and papers.

One common characteristic for the types of wireless sensor networks considered in this thesis is the requirements for self-sustainability. When considering wireless sensor networks in general it is not a strict requirement that the nodes need to be self sustained, a typical indoor network may, for example, very well be tied directly into the electrical grid of the house and thus not be required to take energy considerations into account. For the wireless networks considered here it will henceforth be assumed that the nodes are considered self sustained in energy and therefore have stricter design requirements concerning the overall energy consumption of the device.

2.1 Different Types of Wireless Networks

As was previously stated the main purpose of a wireless sensor network is to relay information between different points, or nodes. However, in the same way that the decisions and actions taken by nodes acting upon this information can vary immensely from one application to another, so to can the way this information is distributed vary. Therefore wireless sensor networks are typically divided into several subgroups, each with its own special structure. A complete overview of all types of wireless networks are not given in this thesis but instead a few general groups of network structures are presented which are used in the work presented in the following chapters. For the interested reader, further references can be found in [7].

2.1.1 Wireless Sensor Networks (General)

The general, and somewhat diffuse, form of wireless networks typically consists of one or more sensor and one gateway. The data collected by the sensors are send to the gateway which either relays the data further or act upon it directly. Several different topologies of sensor networks are available but the main topology which are used in the work presented within the thesis are a star-topology. In this topology the nodes uses a direct link to the gateway, no information are relayed through other nodes. The main reason for using this topology in the work presented in the thesis is the fact that all nodes of the designed networks are located fairly close to the gateway and can thus be assumed to have a direct channel between the sensors and the gateway.

2.1.2 Wireless Body Area Networks

Wireless Body Area Networks (WBANs) can be considered as a subgroup of Wireless Personal Area Networks (WPANs). The definition of WPANs are defined in IEEE 802.15[5]. The main difference between a WBAN and WPAN is that the nodes in WBANs are operating directly in vicinity of the body. A WBAN does not include fixed sensor nodes installed in the surrounding environment.

Wireless Body Area Networks have additional performance challenges as they can be assumed to be in a mobile environment. As such, the performance of a body area network can change as the user moves through different surroundings or simple changes the pose, thus affecting factors such as path of propagation and nearby structures coupling to the wireless devices. Although an environment for a WPAN can change as well, most cases could be assumed to have a relatively slow changing environment.

2.2 Typical Building Blocks

The typical building blocks for a wireless sensor can be seen in Figure 2.1. Regardless of the intended application of the wireless network the following building blocks can usually be found in the device.

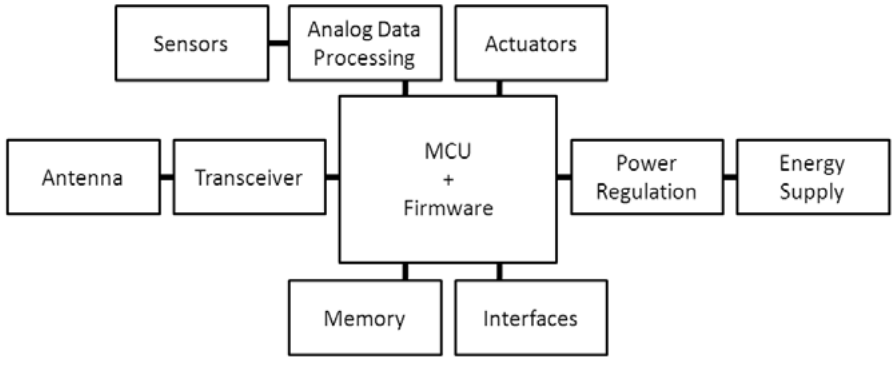

Figure 2.1. Topology of typical WSN node

The microcontroller (MCU) with corresponding firmware is the heart of the circuit and connects to all other peripherals in the circuit. More than often a analog pre-processing of the data provided by the sensors is required in order to fulfill the measurement requirements of the application. This can be, for example, filtering of specific frequency components in the measured data or high precision analog to digital conversion circuitry. The choice of transceiver depends on the protocol and data rates required and hundreds upon hundreds commercial of-the-shelf circuits is readily available which can be tailored for the application. The antenna is also highly dependent on size requirements, radiation characteristics and cost. The energy supply for self sustained wireless devices is usually in the form of a battery but energy generating devices can also be used which generates (harvests) electrical energy from the ambient environment.

2.3 Typical Performance Tradeoffs

Typical wireless nodes are highly constrained devices. Constraints can be either resource constraints (cost, available components, power requirements etc.) or physical constrains (maximum dimensions, weight, bandwidth, etc.). As such several tradeoffs are usually required before a final design can be decided upon. In order to provide some typical tradeoffs which are included in some of the designs presented within the thesis a short list of such tradeoffs is presented below. The tradeoffs presented below can be considered physical (or in other word, unavoidable) tradeoffs.

Operating Frequency vs. Data Rate
The frequency used for wireless transmission is more or less directly dependant on the required data rates. Higher data rates typically requires a wider frequency spectra (bandwidth) and therefore pushes the device to op-

erate at higher operating frequencies. However, at higher operating frequencies the maximum range of the device suffers as the achievable range is better at lower frequencies. This forces the designer to make a tradeoff between data rate, bandwidth related to the operating frequency (fractional bandwidth) and range. An illustration of the required tradeoff can be seen in Figure 2.2.

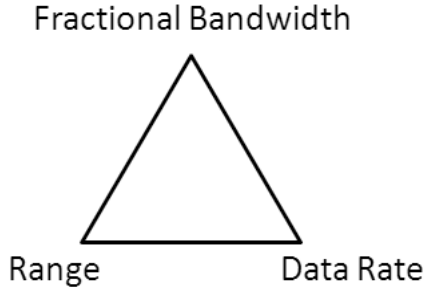

Figure 2.2. Typical tradeoffs for the wireless link

Size vs. Antenna Performance:
As is further covered in detail in section 6 the antenna performance is often strongly linked to the allocated space for antenna placement on the device. In general the tradeoffs can be described as in Figure 2.3. As can be seen, the designer will have to decide between a tradeoff of bandwidth, efficiency and antenna size. A small antenna can generally be efficient (low antenna losses) but then suffers from a low bandwidth (which makes the device sensitive to objects located close to the sensor and limits the data rate) or wideband (can cover a large frequency range and is less sensitive to the environment) but with low efficiency (considerable losses in the antenna). The exact amount of tradeoffs required depends on the physical size and the operating frequency used (the electrical size of the device).

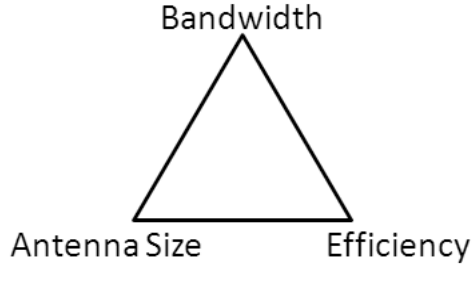

Figure 2.3. Typical tradeoffs for the antenna design

Size vs. Available Power

Power is another crucial resource for wireless nodes. As the size decreases so does the volume available for energy storage and/or generation. If the size of the node was limited only by the size of the circuitry required, wireless devices could be made very small indeed. However, in the real world power requirements further limits the minimum size of the device. If a high performance device is required (high computation capabilities and high data rates) the power consumption goes up. In order to function over a reasonable amount of time a corresponding amount of power is required. It is therefore in general a direct tradeoff between device performance, device size and available power. As seen in the Figure 2.4.

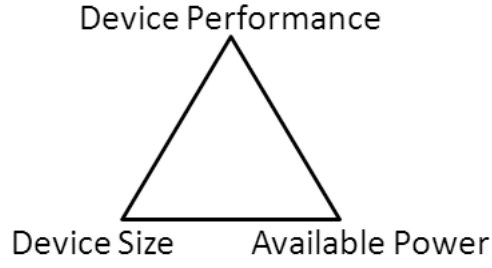

Figure 2.4. Typical tradeoffs between power consumption, available power and device size

3. Wireless Body Area Networks

Wireless Body Area Networks (WBANs) can, as was previously stated, be described as a number of closely linked body worn sensors conveying sensor data wirelessly between them. The initial work which subsequently relates to more or less all other work presented in the thesis started with a body worn sensor system developed for motion monitoring of test subjects. A full description of the major components in the designed system can be found in the original master thesis [6]. However, some of the basic components will be described here to give a view of the full system and to help describe the work which was performed on the system in the time after the initial work presented in the master thesis. Some of the later work was presented at pHealth Oslo and is covered by [PAPER X].

3.1 First Iteration Body Area Network

The first iteration of the body area network was based around a WBAN which gathered accelerometer and temperature data which was then relayed wirelessly to a remote server using a GPRS connection. This allows the test subject to be monitored remotely. The system was developed together with the Swedish Defence Research Agency (FOI) in order to evaluate if WBAN systems could be used for remote soldier monitoring.

3.1.1 Initial System Overview

The developed WBAN system can be described schematically as in Figure 3.1. A worn embedded Linux server serves as the gateway with wireless sensor nodes being connected using the ZigBee protocol. The embedded server gathers accelerometer data, temperature and GPS position and sends the data to a remote server using a GPRS connection.

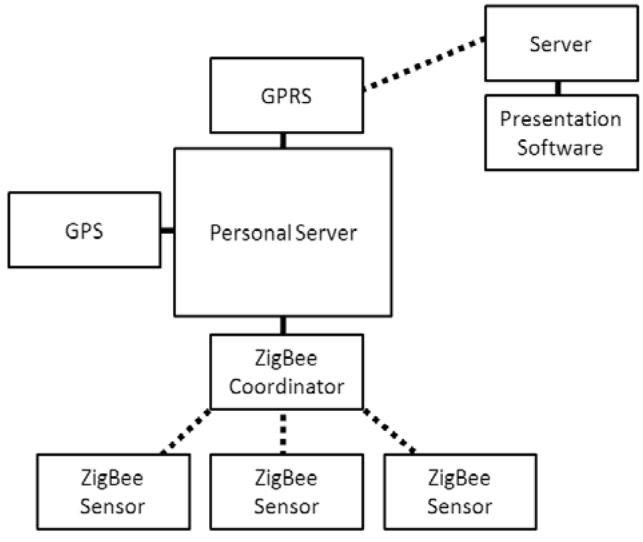

Figure 3.1. Topology of first iteration WBAN system

In order to provide a mean to interpret the accelerometer data and give information about the movement of the test subject two different approaches were tested and evaluated. In the first version a kinematic model of the human body was developed [6] which gave the ability to translate the accelerometer data to limb positioning. In order to model the upper body motion of the test subject a system comprised of 5 3-axial accelerometers were used. The accelerometers were mounted on the torso and the elbow joints of the test subject streamed data continuously to a local server.

Using a model based on inverse kinematics the system could transform data from example the elbow sensors to a measure of the bending angle of the elbow joint. The total collected data could then be used to model the position of the test subject as presented in Figure 3.2. This gave an accurate estimate of the test subject position. However, due to the number of variables given by the accelerometer sensors compared to the variables required for a full solution on degree of freedom could not be determined (one variable could not the solved for due to the high number of degrees of freedom in the shoulder joint) which allow some ambiguity in the system. This is described in further detail in [6].

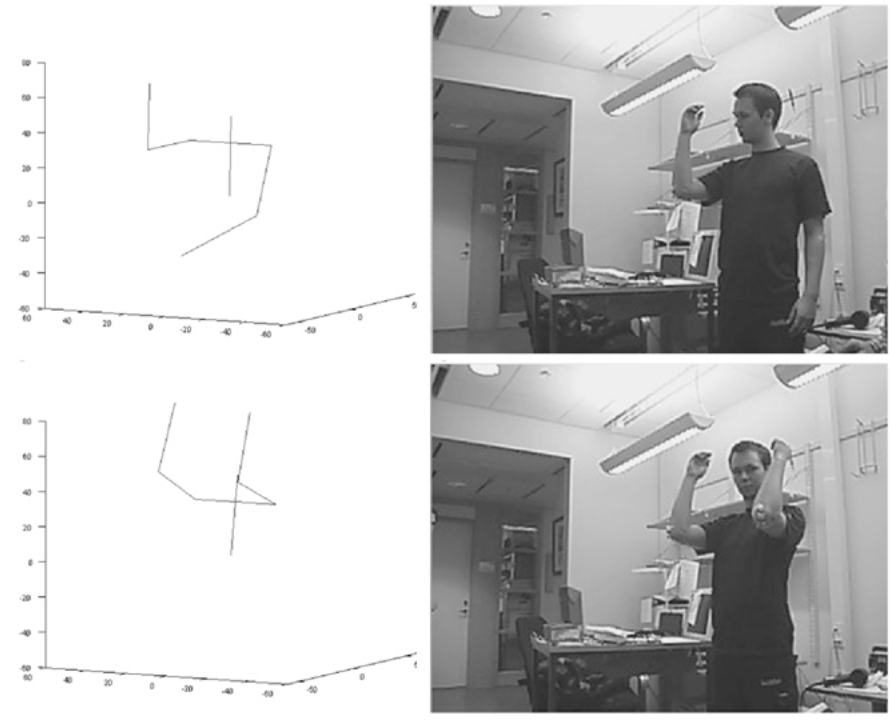

Figure 3.2. Test and data visualization of first iteration WBAN node. Worn sensor on the right and the corresponding calculated posture on the left.

3.1.2 Second System Iteration

In the second version of the system the multiple accelerometer sensors were replaced by a single accelerometer sensor mounted on the torso of the test subject. Although this system gives less information about the exact movement of the test subject it was deemed that five accelerometer sensor were, at the time, to cumbersome for the system.

The movement of the test subject was estimated from the accelerometer data using a probabilistic method developed by FOI. The data interpretation system was used on the remote server which received the data and used to determine if the test subject was standing, moving or laying down. This, together with GPS data, allowed for remote monitoring of the test subject as movement along a test track was performed [3].

3.2 Body Area Network Field Test

The second iteration WBAN was tested a FOIs facilities in Linköping, Sweden. Using a custom presentation software the system was able to monitor

the movement of a test soldier moving around an outside environment. Accelerometer and GPS data was uploaded using GPRS and post-processed on the server-side in order to determine soldier posture and movement as well as to provide visualization of the data. Further information about the test and results can be found in [3].

3.3 Second Iteration Wireless Nodes

After the two initial iteration of the WBANs additional work focused on developing a second generation wireless node. The first generation nodes used in the presented WBANs were considered to have significant drawbacks in the form of limited memory storage, processing capabilities, interface options and fixed protocol (ZigBee). These drawbacks were remedied in the second generation node.

The overall system layout can be seen in Figure 3.3. In order to provide better node performance the previous microcontroller were switched out to use Microchips PIC24F16 series (16-bit controller) and an external flash-memory was added to the node. The uC were set-up to use a custom developed small operating system (OS) with multithread capabilities which were written by the author. This allowed the node to run multithreaded processes so the node could more seamlessly be adopted with different local processing applications while the network stack were active concurrently.

The ZigBee transceiver was replaced with the TRC104 1Mbps FSK transceiver. This transceiver provided the system with a good, general purpose FSK transceiver while at the same time having a very attractive (low) cost.

In order to provide further interface options a USB interface as well as an expansion header was added. The USB interface used a standard FTDI USB to UART IC with a custom console application running on the uC. This allowed the user to interface directly with a PC and send/read commands to and from the node. A picture of the note interface software can be seen in Figure 3.4. The node application was written using C++ and OpenGL.

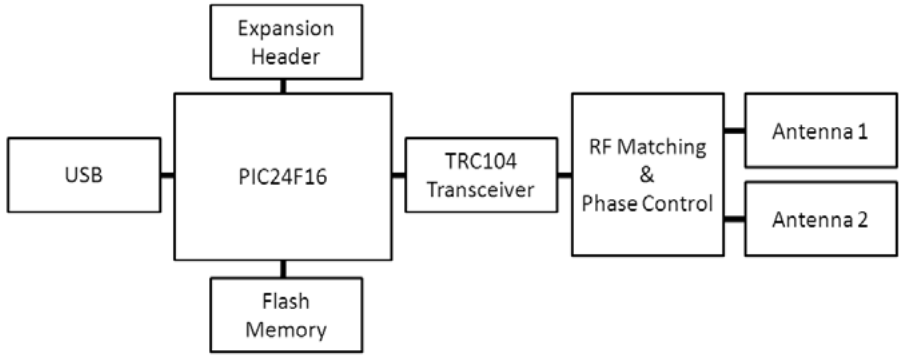

Figure 3.3. Topology of second iteration WBAN node

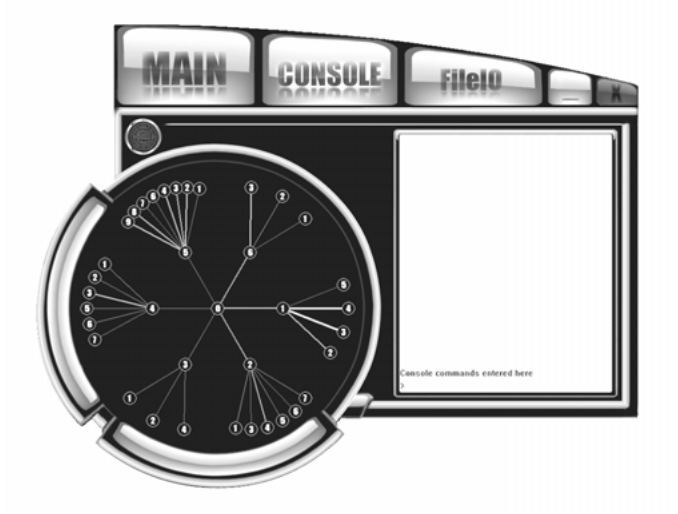

Figure 3.4. Custom GUI for interfacing with connected nodes

In order to provide support for diversity based solutions a simple 90 degree step phase shifter was added connected to the two antenna outputs. This allowed the node to feed the antenna with a relative phase difference of 0, 90, 180 or 270 degrees. The phase shifter used a simplistic approach with LC based phase shifters and discrete RF switches. Due to the limited board space delay line based approaches were omitted and IQ based phase shifters were considered too complex for the target system. However, using a LC based approach gives a limited bandwidth but since the transceiver operates in a very narrow frequency span this was adequate for the application.

The node was layed out as a 4-layer board and the final, mounted version can be seen in Figure 3.5.

Figure 3.5. Manufactured second iteration WBAN node

As can be seen in the figure two short monopole style antennas was integrated around the edges around the node. These antennas were not intended to be used in a fully implemented system but was instead added just to provide a removable on-board antenna which allowed the nodes wireless interface to be tested before installed in custom packaging with different antenna systems.

4. Wireless Sensor Networks in Jet Turbines

Within the scope of the WISEJET project a complete wireless network for real-time monitoring of a running jet turbine was developed. The project was a joint cooperation between Uppsala University, ÅAC Microtec AB and GKN Aerospace Engine Systems - Sweden (formerly Volvo Aero). Within the scope of the project a number of wave propagation measurements in turbine engines were performed in order to allow the wireless network to be designed to cope with the harsh environment within the turbine. The large amount of metal together with moving parts and high temperatures made for a very harsh environment for the wireless system to operate in.

Using measured data from the jet turbine the complete system was adapted, installed and tested in a running jet turbine. The system successfully provided continuous data while the engine was running. Results from measurements are more thoroughly covered in [PAPER III] and [PAPER VI].

4.1 Turbine Environment

The jet turbine consists of an air channel with several stages of rotating blades which channels and compresses the air as it is moved through the engine. Since the engine itself and all blades are metallic and moving at high velocities the turbine environment creates very strong variations in the path-losses between the sensor-nodes and the gateway.

In order to properly evaluate the electromagnetic environment inside the turbine a probe fed by a signal generator was placed at strategic locations inside the fan stage of the turbine and a receiving antenna in front of the engine inlet. The engine and corresponding fan blades were then allowed to rotate and the time behavior of the received signal was recorded. Two types of structures were measured and evaluated, the first was a half scale model of the fan stage of a jet turbine which was borrowed to Uppsala University courtesy of GKN Aerospace. This allowed for a large number of controlled measurements to be taken in the local lab environment. A picture showing the half scale model used can be seen in Figure 4.1. In the figure the three different probe positions used can be seen.

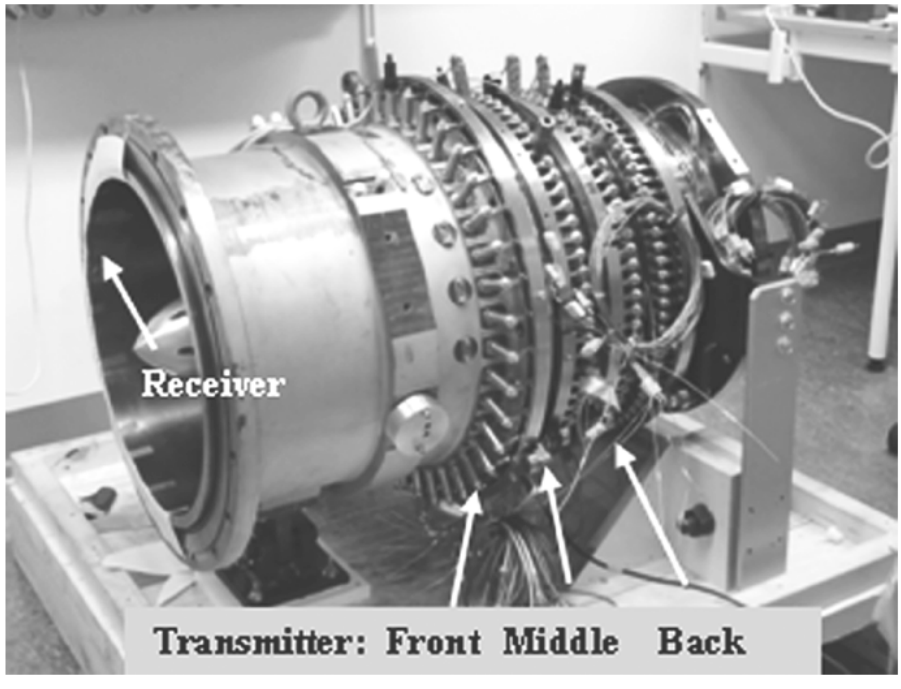

Figure 4.1. Test-setup of half scale jet turbine for EM propagation measurements

The other set of measurements were done at GKNs facilities in Trollhättan, Sweden on a full scale RM12 engine. The RM12 engine is a jet turbine used in the Swedish fighter plane Jas 39 Gripen and is a military grade engine. A descriptive figure of the engine can be seen in Figure 4.2. This allowed for measurement in the final intended environment and also provided a second set of data which could be compared to the first set gathered from the half scale model.

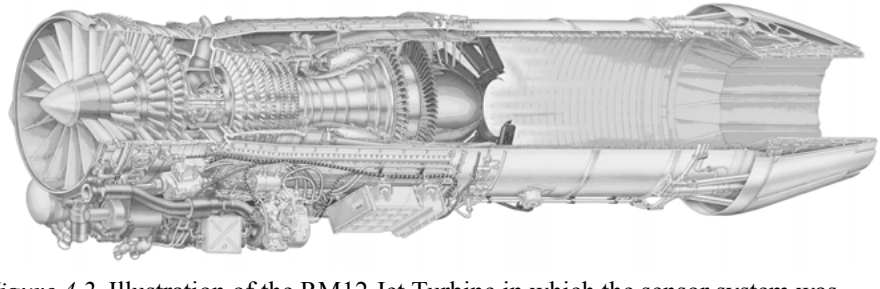

Figure 4.2. Illustration of the RM12 Jet Turbine in which the sensor system was installed.

4.2 System Design & Evaluation

A general description of the developed system can be seen in Figure 4.3. The system uses several wireless nodes which gather information about engine temperature and strains which were then relayed wirelessly to a remote server. The sensors were placed directly in the fan stage of the engine and rotated along with the fan blades. This required the system be able to handle substantial applied forces as well as the high temperatures within the engine. The gateways receive antennas were placed at the inlet of the turbine.

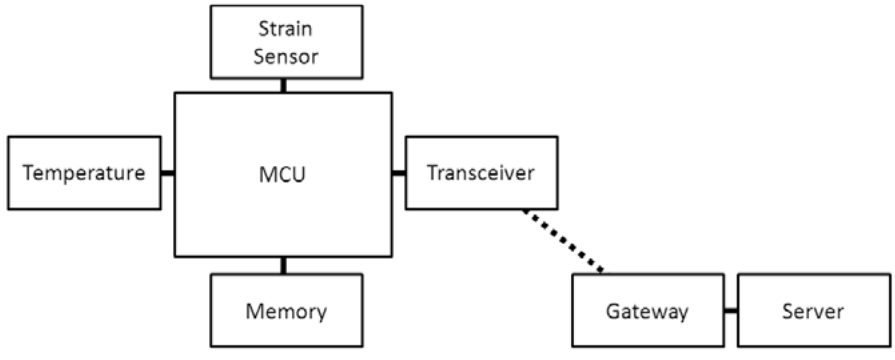

Figure 4.3. Topology of turbine WSN system

A large number of propagation measurements were performed in both the full scale engine and the half scale. The measurements showed severe fading which were a direct function of the blade position inside the fan stage. As the engine is a highly symmetric system the only unique variation in signal strength appears as the blades shift position in one incremental step. An example of the measured fading variations can be seen in Figure 4.4. The deep fading nulls can be tracked as a direct function of the number of blades and the rotation speed of the engine.

As can be seen in the figure the fading nulls can be quite severe. The data shown is for slow rotation speeds of 60 rpm but, due to being a direct function of blade position, can be scaled up to full engine speed. At full engine speed the time between the consecutive fading nulls were estimated to roughly 120 μs. This meant that the system needed to be designed in such a way that it would still have a high likelihood of successfully transferring the data packages under these conditions.

Considering the short time span between the fading nulls amplitude modulation (AM) was deemed unsuitable for the system. The reason behind this was that the extremely fast rise and fall times in the signal amplitude close to the fading nulls were considered a risk for successful package transfer, especially by interfering with the transceivers Automatic Gain Control

(AGC). Instead the system adapted frequency shift modulation (FSK) as the modulation form of choice. Also the package length was kept short and the data rate high in order to reduce the number of fading nulls during each package.

The transmit antennas for the sensors embedded within the turbine were based on standard patch antennas which were manufactured using a thin 0.1 mm substrates in order to be able to place the transmit antennas conformably on the blade surface. However, some reductions in efficiency of the transmit antennas were experienced due to size limitations and the required thickness of the substrates.

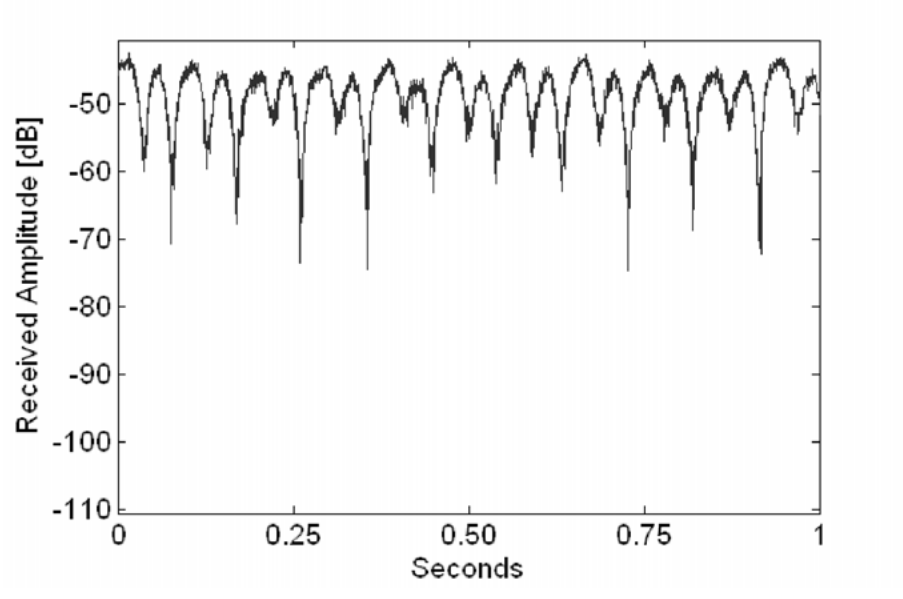

Figure 4.4. Typical fading characteristics in jet-turbine environment

In order to test the overall system and evaluate if the chosen transceiver (and corresponding modulation and package structuring) could be deemed suitable for the final on-site testruns a simulated enivronment for testing was set-up. The setup comprised of the manufactured test nodes, a Keithley spectrum analyzer used for recording transmitted packages, a PC running matlab for processing recorded packages and a Keithley signal generator for playing back recorded and modified packages.

Using the setup real-life packages could be successfully recorded and superimposed with measured propagation channel measurements which were scaled up to various engine speeds. This allowed for testing of several operating conditions including package-length, data encoding, engine rotational speeds and overall channel losses. An example sequency can be seen in Figure 4.5. In the figure recorded data is shown before and after the measured fading sequences were added.

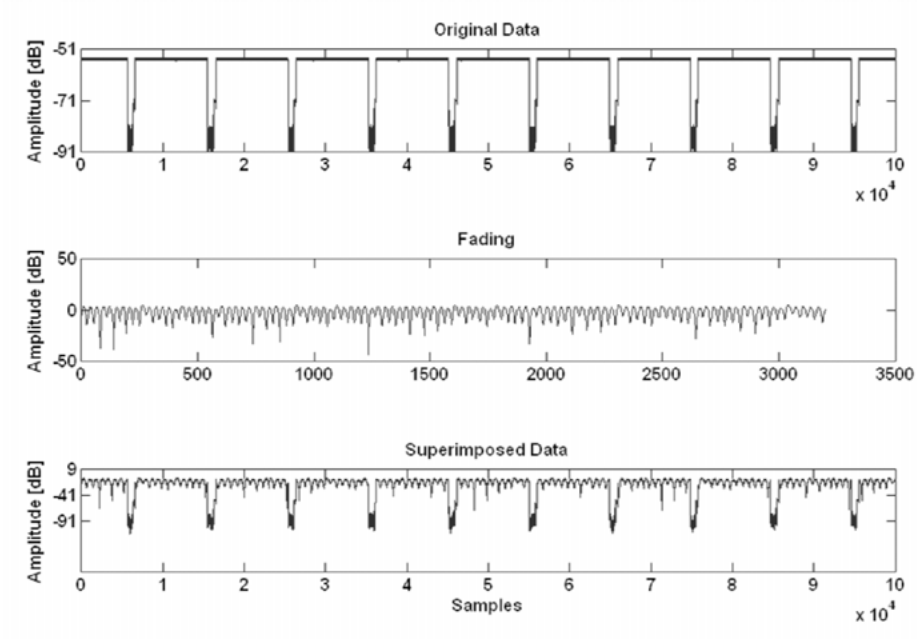

Figure 4.5. Original data modulated by recorded environmental fading and retransmitted using a signal generator

Example performance data for one of the many tested setups is shown in Figure 4.6. In this figure the simulated engine speed was 13 000 rpm, the package payload length was 32 byte and CRC was enabled. The pathloss was then swept in magnitude between 40 to 70 dBm. This was done in order to get data on the expected package-error-rate as a function of the overall losses (antenna losses, matching losses, free-space losses) in the system.

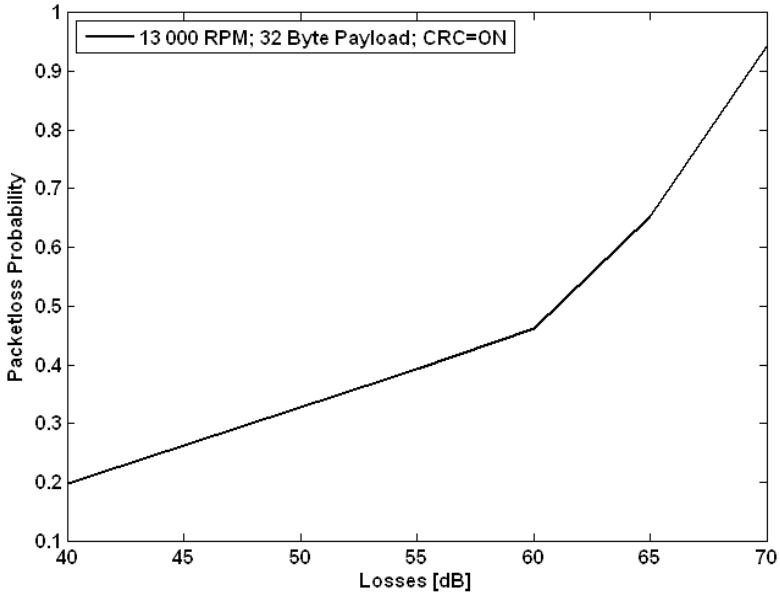

Figure 4.6. Dropped packages in real receiver reading emulated turbine data

4.3 System Performance Test

The complete system was tested at GKNs test facilities in Trollhättan, Sweden. In these tests live data was recorded on a running, full scale RM12 engine. Due to the high costs involved in setting up the test only one full scale test were performed. The maximum rotational speed of the live tests were restricted to 2000 rpm. The system successfully recorded and transmitted temperature data during the test and an example of recorded data can be seen in Figure 4.7.

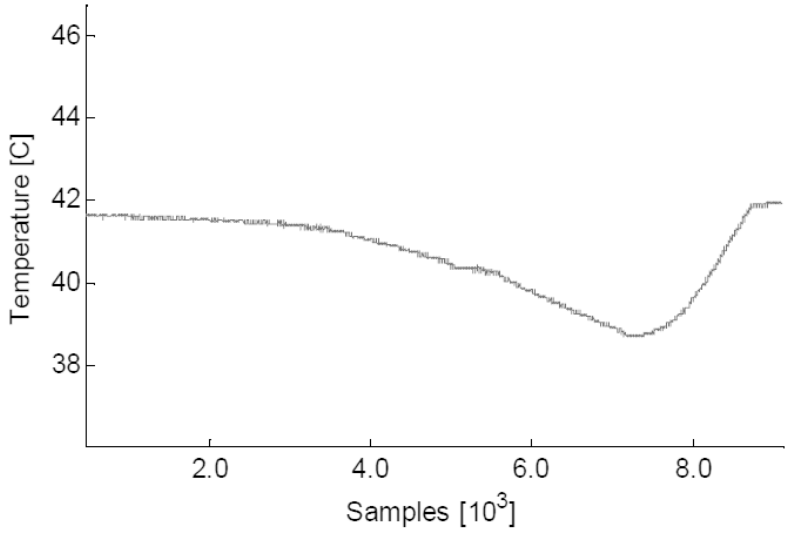

Figure 4.7. Temperature measured live in running jet turbine

4.4 Modeling of Turbine Environment

After the bulk of the project and the corresponding full scale tests had been performed some work continued on trying to further understand the propagation environment inside the turbine. In order to try to find a way to understand and model the environment a simplified model based on the same fundamental principles as was used in early modeling of whispering gallery modes were used. A short version is covered in [PAPER IV] but are given more detail in the following sections.

4.4.1 Introduction

Since the exact geometry of a turbine engine is extremely complex as well as a highly protected trade secret a simplified structure was investigated in order to provide a basic model. The model used is shown in Figure 4.8. The model is very similar to that of a very large (electrically) coaxial transmission line. The model comprises of two conducting cylindrical layers (outer and inner layer) with an air channel in-between where the signals propagate. The major difference between the simplified model and that of a real-life engine is that the model do not have the corresponding fan blades or radial variances along the axial. It was decided that a simplified model were to be evaluated first to see if the model held up before further details were included.

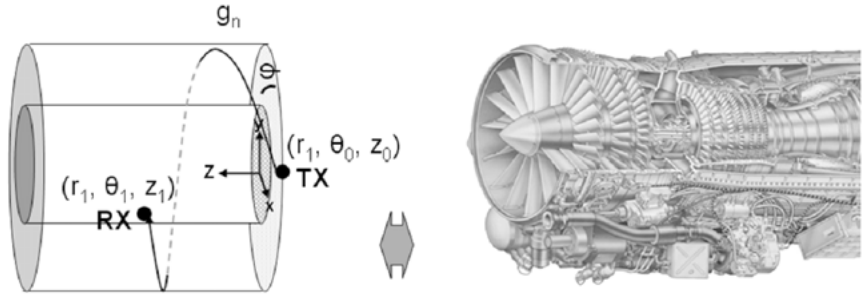

Figure 4.8. Simplified model of jet-turbine

Based on the simplified structure the average power distribution inside the structure was calculated using an analytical model based on the superposition of propagating helical rays in the structure. This is very similar to what was done in the first whispering gallery mode models developed for circular structures with the major difference being that the modelled structure is cylindrical rather than planar.

The standard solution to obtain the field distribution in such a structure would be to attempt a direct application of Maxwell's equations with the Laplace equation described in cylindrical coordinates to solve the problem. However, due to fact that the environment is severely overmoded as well as not being entirely in the far-field region a simplified approach is used here.

It is important to note here that the goal was to investigate if modelling the propagation as a sum of superimposed helical rays would yield a power distribution which corresponded to measurements and in this way help validate if this would be a valid way to illustrate how the measured power distribution is formed. It is *NOT* the purpose to provide an alternative way to solve EM problems instead of using Maxwell's equations, it never was and will never be.

4.4.2 Model

From the radiating antenna, the rays can propagate along the structure in two rotational directions, right and left hand. The propagating waves in the cylinder is modelled as following,

$$f_1(r,\theta,z) = r_1\hat{r} + ct\cos(\varphi)\hat{\theta} + ct\sin(\varphi)\hat{z} \tag{4.1}$$

$$f_2(r,\theta,z) = r_1\hat{r} - ct\cos(\varphi)\hat{\theta} + ct\sin(\varphi)\hat{z} \tag{4.2}$$

where r_1 is the radius of the hollow layer and φ is the pitch of the helical curve. A fix radius r_1 is used in the model. Although r_1 does in fact have a span between a maximum and minimum value the same motivation for using a fix radius is used as that used to determine the approximate cutoff frequency of a coaxial waveguide. In a coaxial waveguide the cutoff frequency can be related to the average radius at which the total circumference inside the structure is equal to one wavelength. This is the standard form commonly used to approximate the k_c of a coaxial waveguide and the same average radius r is used in this model.

In order to derive the total power received at a location (r, θ, z) all the possible rays f_1 and f_2 passing through this point must be calculated. This will yield an infinite discrete number of φ_n which makes f_1 and f_2 pass through the desired point.

Each possible φ_n which creates a unique path through (r, θ, z) must have a corresponding unique time of travel t_n (and corresponding phase shift). Each path must have travelled n rotations around the structure which yields the following curve parametrics

$$\theta = \theta_1 + 2\pi n = ct_n \cos(\varphi_n) \tag{4.3}$$

$$t_n = \frac{\theta_1 + 2\pi n}{c\cos(\varphi_n)} \tag{4.4}$$

$$z = z_1 = ct_n \sin(\varphi_n) \tag{4.5}$$

$$t_n = \frac{z_1}{c\sin(\varphi_n)} \tag{4.6}$$

Equating (4.4) and (4.6) yields

$$\frac{z_1}{\theta_1 + 2\pi n} = \frac{\sin(\varphi_n)}{\cos(\varphi_n)} = \tan(\varphi_n) \tag{4.7}$$

Equation (4.7) gives all infinite discrete paths from n=0 to n=∞ which goes through (r, θ, z).

Once the set of curves going from the transmitting point $(r_1, 0, 0)$ to the receiving point (r_1, θ_1, z_1) has been found the corresponding arc-lengths can be calculated as

$$\mathbf{L}_{1n}(r, \theta, z) = (\theta + 2\pi n)\sqrt{r^2 + \left(\frac{z}{\theta + 2\pi n}\right)^2} \tag{4.8}$$

$$\mathbf{L}_{2n}(r,\theta,z)=(2\pi(n+1)-\theta)\sqrt{r^2+\left(\frac{z}{2\pi(n+1)-\theta}\right)^2} \tag{4.9}$$

It important to note that in the case of n=0 and θ =0 the z-term in L_{1n} is divided by zero and at n=0, θ =2π the z-term in L_{2n} is divided by zero. In both cases the limiting value of L_{1n} which goes to z should be taken.

In order to describe the total number of propagating waves that superimpose at a point with coordinates (r, θ, z) the propagating waves are described as

$$g_{1n}(r,\theta,z,f,t)=Ae^{-\gamma L_{1n}}\sin\left(2\pi ft+\frac{2\pi fL_{1n}(r,\theta,z)}{c}\right) \tag{4.10}$$

$$g_{2n}(r,\theta,z,f,t)=Ae^{-\gamma L_{2n}}\sin\left(2\pi ft+\frac{2\pi fL_{2n}(r,\theta,z)}{c}\right) \tag{4.11}$$

Where A is the amplitude, γ is a dampening factor and f the frequency. The instantaneous received power *at* (r_1, θ_1, z_1) can be calculated by summing the total number of curves as

$$h(r,\theta,z,f,t)=\sum_{n=0}^{\infty}\left[g_{1n}(r,\theta,z,f,t)+g_{2n}(r,\theta,z,f,t)\right] \tag{4.12}$$

An analytical form for the sum expressed in equation (4.12) has not been found which means that the number of rays must be capped in order to be able to calculate the sum. This is done by rewriting (4.12) as

$$h(r,\theta,z,f,t,N)=\sum_{n=0}^{N}\left[g_{1n}(r,\theta,z,f,t)+g_{2n}(r,\theta,z,f,t)\right] \tag{4.13}$$

Where N is the total number of rays summed. In order to get a valid result from equation (4.13) the dampening factor γ must be large enough to allow the solution to converge.

Equation (4.13) gives the instantaneous signal amplitude at (r_1, θ_1, z_1), in order to calculate the average received signal an average during one period is calculates as

$$k(r,\theta,z,f,N)=\frac{1}{T}\int_0^T\sqrt{h(r,\theta,z,f,t,N)^2}\,dt \tag{4.14}$$

Using equation (4.14) the average received power as a function of position and frequency can be plotted.

Determining a suitable value for N was done by using a root mean square error (RMSE) calculation to evaluate the number of rays required for the solution to converge to a stable value. The RMSE was calculated using two different estimates, 1) an upper bound for the highest possible RMSE value given a certain N and 2) the calculated distribution of the largest N simulated. The resulting RMSE plot is seen in Figure 4.9. The RMSE value was calculated as

$$RMSE = \sqrt{\frac{\sum \left(k(\theta,z) - k_{ref}(\theta,z)\right)^2}{n}} \tag{4.15}$$

where n is total number of simulated points. In order to provide a way of ascertaining if the selected N is "large enough" an upper bound for the maximum RMSE value was derived. Without this bound the solution provided by equation (4.14) would have to be iterated over an increasing number of N in order to make sure the solution has (seemingly) converged. The basis for the upper bound is determined as follows.

Due to the dependence on sinusoidal components a closed form for the expression presented in equation (4.13) has not been found. Therefore the sinusoidal components in equation (4.13) are neglected and only the exponential terms are kept. Summing over all remaining exponential terms in the range [N, ∞] provide the maximum error possible if all remaining terms were to add in-phase. The sum can be described as:

$$\Delta = \frac{A}{\sqrt{2}} \sum_{n=0}^{\infty} \left(e^{-\gamma_{1n}} + e^{-\gamma_{2n}} \right) - \frac{A}{\sqrt{2}} \sum_{n=0}^{N} \left(e^{-\gamma_{1n}} + e^{-\gamma_{2n}} \right) \tag{4.16}$$

the amplitude A has been divided by the square root of 2 in order to match to the RMS value calculated in equation (4.14). Likewise equations (4.8) and (4.9) fulfil the following

$$\mathbf{L}_{1n}(r,\theta,z) \geq 2\pi nr \tag{4.17}$$

$$\mathbf{L}_{2n}(r,\theta,z) \geq (2\pi - \theta) nr \tag{4.18}$$

And, if n >>1, will actually converge to these values. Using the right-hand side of equations (4.17) and (4.18) in equation (4.16) will provide a maximum remaining error which can, using standard summation identities, be simplified to

$$\Delta(\theta) = \frac{A}{\sqrt{2}}\left(e^{-\gamma\theta r} + e^{-\gamma(2\pi-\theta)r}\right)\left(\frac{1}{1-e^{-2\gamma\pi r}} - e^{-2\gamma\pi r}\left(\frac{e^{-2N\gamma\pi r}-1}{e^{-2\gamma\pi r}-1}\right)1-1\right) \tag{4.19}$$

Using equation (4.19) the largest possible k if all neglected terms were to add in-phase can be described as

$$k(\theta,z)_{\max} = k(\theta,z) + \Delta \tag{4.20}$$

where r, f, N in equation (4.14) are assumed to be fixed. Combining equation (4.15) and equation (4.20) yields an upper bound on the form

$$RMSE_{\max} = \sqrt{\frac{\sum(\Delta(\theta,z))^2}{n}} \tag{4.21}$$

In order to obtain a reasonable selection of γ for the propagating rays the loss tangent for a fixed height, infinitely broad parallel plate waveguide is used. This is an approximation motivated by the relatively large (electrically) radius of the structure defining the path seen by the travelling wave between the inner and outer layer. The loss tangent of a parallel plate waveguide in vacuum whose width goes towards infinity can be described as

$$\gamma = \frac{2R_s}{d\eta} \tag{4.22}$$

where R_s is the sheet resistivity, d is the spacing between the plates and η is the impedance of freespace. The setup used for measurement validation is constructed out of T304 austenitic stainless steel. For simulations a relative permeability of 1.008 and a resistivity of 7.2e-5 Ωcm are used yielding a sheet resistivity of 0.24 Ω/□ at 10 GHz. This gives $\gamma = 0.032$. The model uses a conductor spacing of 40 mm.

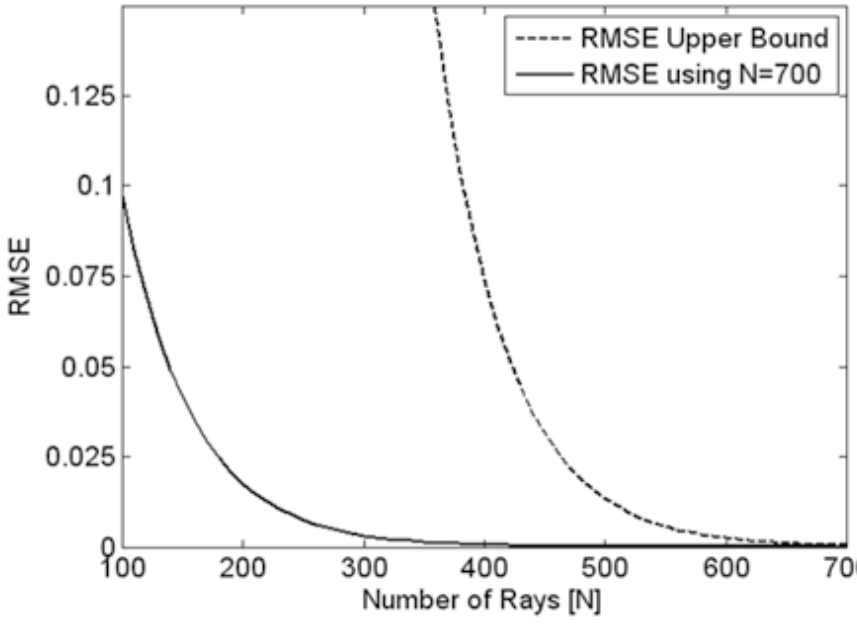

Figure 4.9. Calculated RMSE based on both simulated data and upper bound

4.4.3 Simulations & Measurements

In order to compare measured and calculated results a setup was designed which corresponded to the calculated model. The resulting setup can be seen in Figure 4.10. The constructed setup has been electrically scaled in order to be able to physically manufacture the setup within a reasonable budget. The structure was scaled to roughly a quarter of the size of an RM12 engine and simulations, calculations and measurements were performed at 10 GHz (corresponding to 2.45 GHz in the RM12 sized engine).

In order to provide a number of the RMSE the model was simulated using 100 to 700 rays and plotted as in Figure 4.9. The calculated upper bound RMSE can also be seen in the same figure.

Using the measurement setup described in Figure 4.10. the power distribution inside the structure was measured. The data was measured using a small monopole probe which probed the inside of the cavity in 1 cm steps. The TX probe was placed on a rotating sleeve at the edge of the setup and rotated in 1.5 degree steps. A signal generator fed the transmitting probe and the receiving probe was connected to a spectrum analyzer.

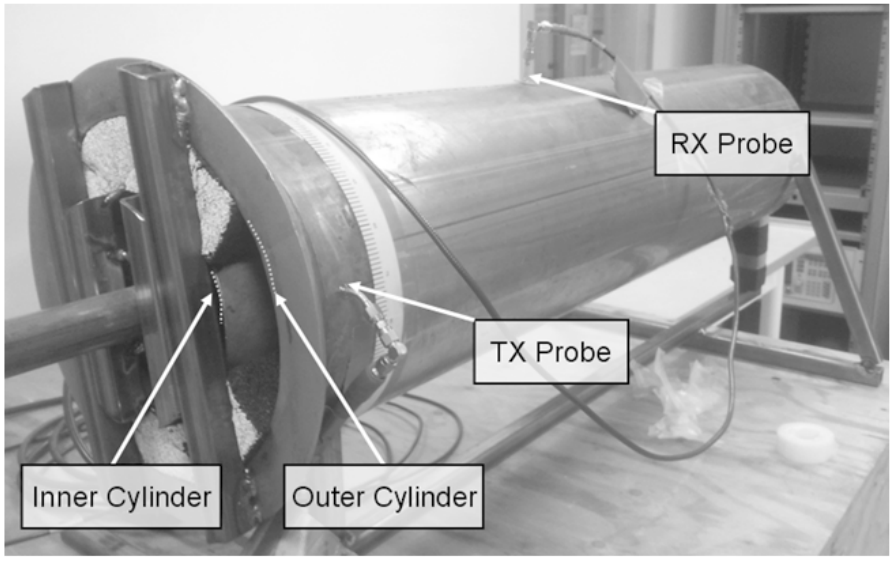

Figure 4.10. Measurement setup used to compare mathematical model with real data

Two areas were probed, each measuring 10 cm and going from 0 to 180 degrees. 180-360 degrees was not measured due to symmetry but a few measurements were done to verify that the setup was indeed symmetrical. The distances measured were 10-19 cm and 50-59 cm. The two measured areas contain in total 2400 measurement points. Figure 4.11. and Figure 4.12. shows the calculated, measured and simulated results.

In addition to measured and calculated values the structure was simulated using CST Microwave Studio. However, due to the fact that the structure is relatively high Q-valued as well as electrically large (1 m long at 10 GHz) the simulated results show the strongest deviation from measured values. As all surfaces in the model is curved a very high mesh density was required but the maximum mesh density the simulation PC could handle (due to memory constraints) would ideally be able to be set even higher to give more accurate simulation values. The presented values in Figure 4.12. was with the highest mesh density settings the PC could handle.

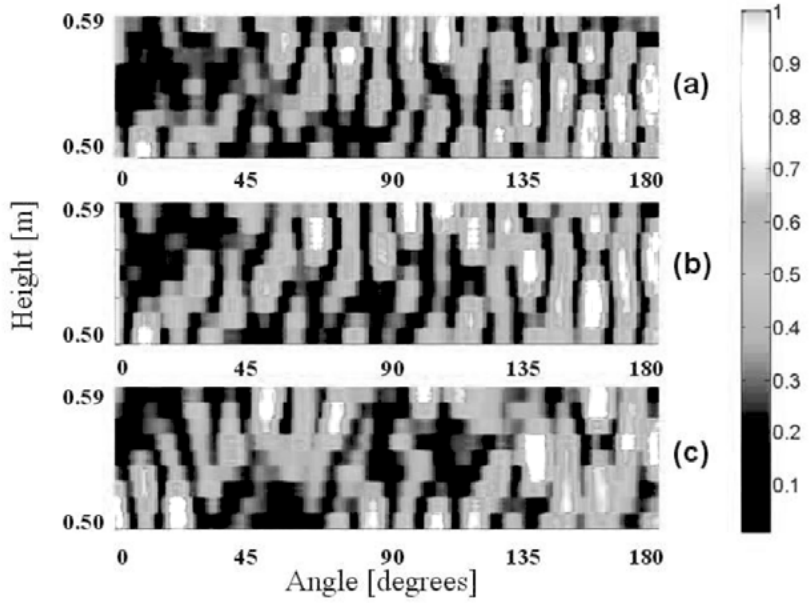

Figure 4.11. Data covering 50-59 cm into the structure. a) Measured values, b) Simulated values in Matlab based on model, c) Values obtained using CST Microwave Studio

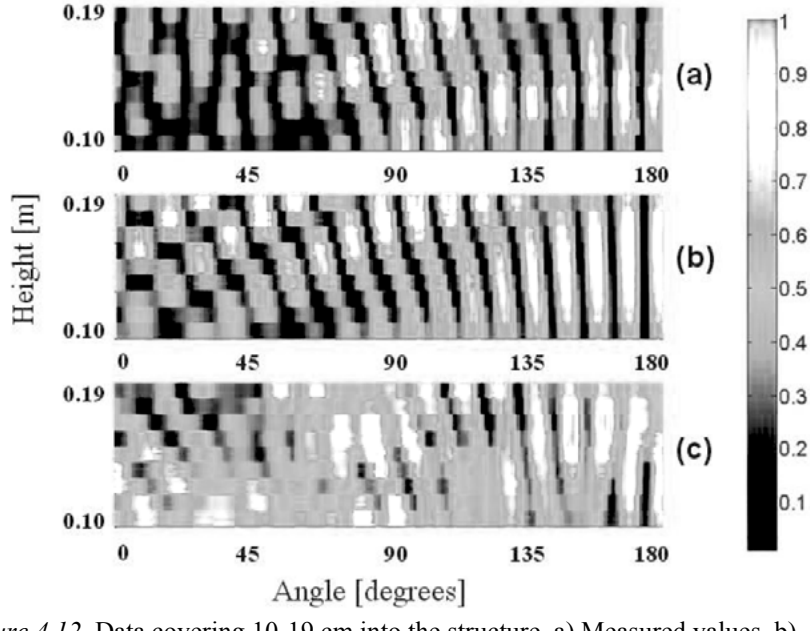

Figure 4.12. Data covering 10-19 cm into the structure. a) Measured values, b) Simulated values in Matlab based on model, c) Values obtained using CST Microwave Studio

5. Diversity Combining for Wireless Sensor Networks

Wireless nodes are often operated in environments where a lot of external reflective surfaces are present. This causes the average power distribution of a transmitted signal to vary greatly at different locations across the environment. If a node only has a single antenna element these variations can cause significant degradation of the overall node performance.

In order to make the node more robust to these kinds of environments different tactics can be used, one such tactic is to provide the node with multiple antenna elements which can be used for transmitting and receiving. If the different antenna elements can be considered uncorrelated then each antenna element will experience an individual distribution of these signal strength variations as the environment around the node changes. This provides the node with a way to have several receive signals which vary in signal strength more or less independently from each other. By either choosing the antenna element with the strongest signal or by combining the different receive signals the node can obtain a much better (diverse) average performance. This chapter is based around the data presented in [PAPER II] and [PAPER IX]

5.1 Diversity Combiner Schemes

A large number of different types of schemes can be used to combine the different receive signals before relaying the signal to the receiver. This thesis will not consider all these different types of diversity schemes but instead reference to the section written in [7] and [PAPER IX]. However, one example of the simplest type of diversity combiner is given. In Figure 5.1. a schematic view of a selection combiner is shown. In this type of diversity receiver the input signal from multiple signal sources (receive antennas) is monitored and the receiver switches between the elements in such a manner that the highest strength signal is always chosen.

In this thesis the focus will be on using varying phase sweep architecture to provide a more robust average signal, generally designated as *Phase Sweep Diversity*.

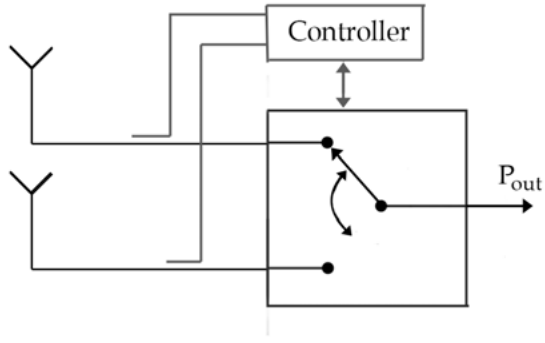

Figure 5.1. Schematic view of diversity selection combiner

5.2 Discrete Phase Sweep Transmit Diversity

5.2.1 Introduction

Data for the first prototype system designed was presented by the author at the European Microwave Week in 2009, Barcelona. [PAPER II] proposes the use of multiple phase shifted signal combinations per symbol without a feedback network, in order to facilitate a minimum component diversity switching technique The effect of both a peak detector system and a system with an averaging detector were investigated. Simulations and measurements in both reverberation chamber and office environment were presented that supporting the use of the proposed technique in ASK systems.

The initial prototype was designed for 433 MHz, the reason to design the prototype for a fairly low operating frequency (compared to the many existing systems operating on 2.45 GHz) was mainly to relax the design requirements needed to ensure that the systems switch electronics was fast enough compared to the data-rate as well to reduce the effects of transmission line lengths between subcomponents. A simplified schematic of the switch can be seen in Figure 5.2.

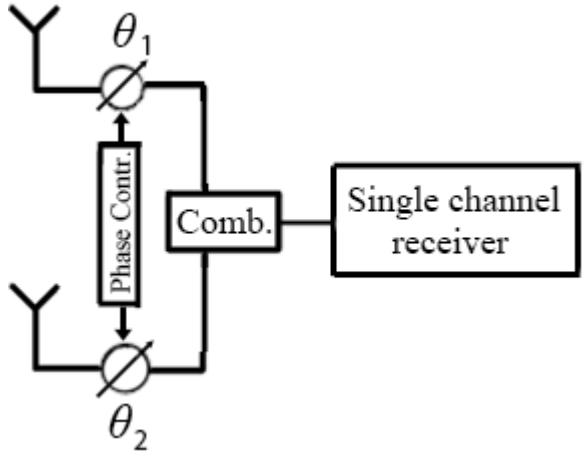

Figure 5.2. Schematic view of phase sweep diversity combiner

Designed as a proof of concept there was a few important assumptions that were made to this design, mainly; 1) The two antenna elements was assumed to have zero mutual coupling, relaxing the requirements of having to take into account the effect of antenna detuning due to mutually induced currents on the elements, 2) The power requirements of the prototype switch was not of primary concern, 3) The switching noise was not considered and 4) The potential spectral broadening due to the high switching speed did not matter. All these assumptions simplified the prototype design but needs to be kept in mind when considering the complete system.

When designing the system three types of RF switches were considered, PIN diodes, MEMS switches and FET based switches. Considering the types of switches appropriate for the combiner design the use of MEMS switches was deemed less suitable. The reason not to use MEMS switches in the design was due to the high switching speeds required. As the system needs to switch through the various phase-shift combinations faster than the symbol rate of the system using hot-switching (switching while the RF-power is turned on) the rated life expectancy for a MEMS switch is quickly reached. For example, at the time of writing the original paper Omron supplied a miniature SMD MEMS switch with a rated life expectancy of 10^8 operations. If a system would have a moderate symbol-rate of 250 kBd the diversity combiner would need to be switching at a minimal of 500 000 switches per second. At this rate the life expectancy of the MEMS switch would be reached in a little over 3 minutes of continuous operating time making the system barely usable. Using limited transmission of data and duty cycling of the device the life expectancy of the system could be increased but it is still the authors opinion that the performance of the MEMS switches currently available is ill suited for this type of operation.

5.2.2 Prototype Evaluation

The prototype system was designed using a simple board with PIN diodes providing a discrete phase sweep circuit. Additional information regarding the prototype board can be found in [PAPER II] and [7]. The performance of the prototype system was evaluated in both a perfectly Rayleigh distributed environment (large reverberation chamber) and an office environment. The system performance in an ideal Rayleigh environment can be seen in Figure 5.3. Two received power levels were recorded and the corresponding output powers for two different types of detector architectures were calculated. The two types of detectors considered was peak detection (always taking the switch configuration that provided the highest input power to the receiving system) and average detection (using the average power of all switch-configurations during the received symbol). As can be seen in Figure 5.3. and Figure 5.5. both type of detector schemes would yield a significantly more reliable received signal.

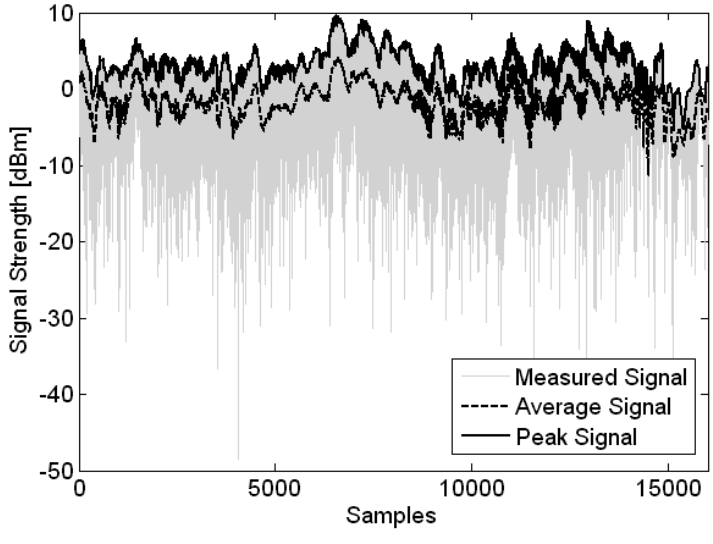

Figure 5.3. Measured signal strength in reverberation chamber and average and peak signal obtainable if using discrete phase sweep diversity

The prototype system was also evaluated in a multiscattering office environment. The variation in signal strength from both the individual antenna configurations and the average signal can be seen in Figure 5.4. Even though the environment could not be expected to posses the same perfect Rayleigh distributed signal as the reverberation chamber the office environment still exhibited large variation in signal strength both as a function of time (spatial displacement) and antenna configuration.

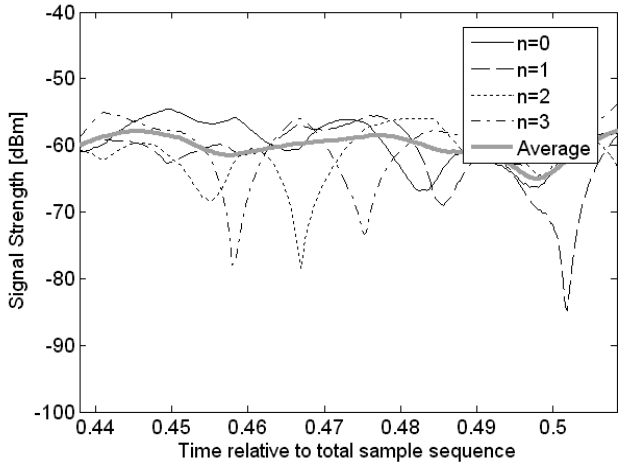

Figure 5.4. Four measured input signals and plotted average signal

The signal strength as the system moved around the office environment was measured and the received signal using both average and peak detection was calculated. The data can be seen in Figure 5.5. Unlike the reverberation chamber environment a slow-fading component can also be seen in the measurement. Both average and peak detector yielded a significantly more reliable system compared to using the system without any form of diversity combiner.

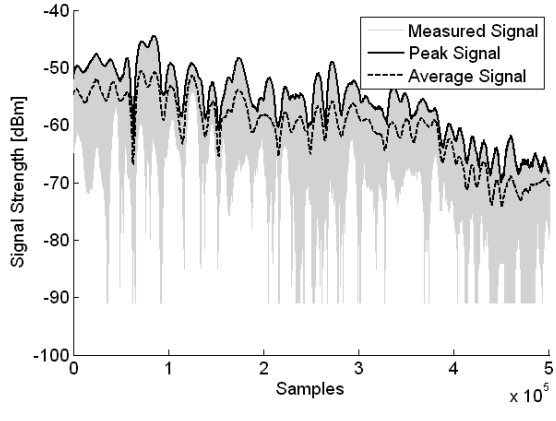

Figure 5.5. Measured signal strength in indoor office environment and average and peak signal obtainable if using discrete phase sweep diversity

5.2.3 Node Design for DPSTD Support

When designing the wireless node described the RF frontend was design to include the hardware required to support DPSTD. An example board of the node hardware used for this wireless node is shown in Figure 5.6. In this figure the phase shift circuitry has been outlined. The implemented phase shifter provides 0, 90, 180 and 270 degree relative phase shift between the two antenna outputs.

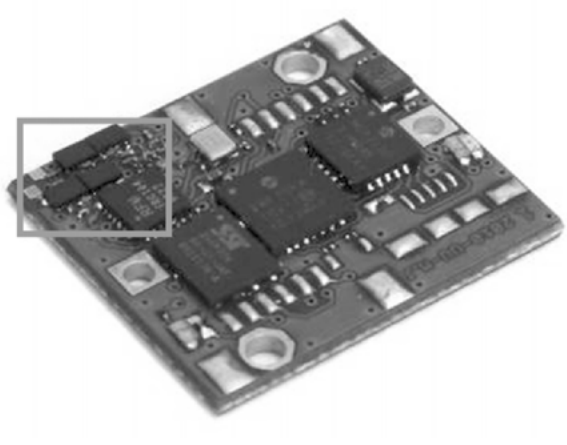

Figure 5.6. Prototype sensor with embedded discrete phase sweep diversity

6. Antenna Design for Wireless Networks

In order to maximize the performance of a wireless node great care must be taken to make sure a properly designed and matched antenna system is used. The considerable size constraints on wireless nodes induce a number of tradeoffs in the design of such antennas. In this section some general primers related to developing node antennas are given together with some general physical limitations on electrically small antennas.

6. 1 Electrically Small Antennas - A Primer

The design of electrically small antennas puts additional limitations on what kind of performance which can be expected from the antenna. An antenna is considered electrically small when the physical size of the radiating structure is small compared to the wavelength. It is important here to note that the actual radiating structure can be much larger than one might initially suspect. Most antennas used in conjunction with commercial wireless transceivers in wireless nodes are unbalanced antennas, this means that the electromagnetic field propagates between the groundplane and the microstrip line/antenna element. This also means that the groundplane is just as important for the antenna performance as the "antenna" itself. Fact is, both these are two parts of the total antenna. By example, in a monopole antenna, the groundplane is just as important for the performance of the antenna as the monopole "whip" itself.

The relationship between groundplane size and antenna performance becomes critical when designing an antenna for a wireless sensor as the overall size of the sensor is generally desired to be as small as possible, this means that the total groundplane for the antenna decreases and, as will be seen in the coming sections, the antenna either becomes less efficient or increasingly narrowbanded. One of the key-points for this section is to highlight the importance of the antenna design in wireless sensors as well as provide some advices important in antenna designs for wireless sensors. This information is important not only for the engineer designing the actual antenna for a wireless sensor but also for anyone using wireless sensornodes as the behavior of the antenna can affect both data-transmission as well as how the node should be handled and placed in the environment. Several of the key points

covered below has been previously mentioned in the licentiate [7] and further information can be found there.

6.1.1 Size Limitations

A good starting point to get an overall grasp of the functioning and performance of antennas in wireless nodes is to be aware of the fact that an electrically small antenna can generally be considered as a RLC resonance circuit. In the same way as the bandwidth of a RLC circuit is related to the Q value the bandwidth of an electrically small antenna can be related to its Q value as well.

Some of the most well known works published concerning the physical limitations of small antennas were done by L. J. Chu [8] and R. F. Harrington [9], their work focused on setting an upper physical limit of how good a small antenna of a certain size could be. Their work was later summaries by R. C. Hansen [10] and modified slightly by Mclean [11] in order to provide a more accurate expression. It should be noted, however, that much of their work are a continuation of the observations made by Wheeler [12].

In the work presented by these authors the performance of the antennas are given in the form of the Q-value of the antenna. The Q-value is defined as

$$Q = \omega \frac{W_m + W_e}{P_{rad}} \tag{6.1}$$

Where W_m and W_e is the average magnetic and electric energy and P_{rad} is the power radiated. In the case of most small antennas the average stored energy can be assumed to be either electric or magnetic depending on the type of antenna investigated. It is important to note here that if the structure contains lossy structures P_{rad} would need to be replaced with a total P_{loss} containing both radiated and other losses. However, in this case the main interest is the optimum performance achievable by any antenna structure and therefore the total structure is assumed to be lossless.

In the work presented by Chu the total volume considered was taken as the smallest imaginary sphere which contains the antenna. Using this definition of the antenna volume an expression describing the lowest possible Q-value was derived. The lower the Q value of a lossless antenna structure the more power is radiated compared to the average stored energy. The final expressions which gives the minimum Q value for a linearly polarized antenna, also including some slight modifications performed by Mclean[11], is given as:

$$Q_{\min,linear} = \frac{1}{k^3 a^3} + \frac{1}{ka} = \frac{1}{8\pi^3}\left(\frac{\lambda}{a}\right)^3 + \frac{1}{2\pi}\frac{\lambda}{a} \tag{6.2}$$

Where k is the wavenumber, a is the radius of the smallest possible sphere that contains the entire antenna structure and λ is the wavelength. Note that this is for a linearly polarized antenna, if the antenna structure is circularly polarized the minimum achievable Q value effectively drops to half that of the linear case. As can be seen from equation (6.2) the minimum Q-value as a function of wavelength and radius a rises steeply when the physical dimensions of the antenna gets small compared to the wavelength.

When specifying the electrical size of an electrically small antenna the antenna's *ka* value is used. Where k is the wavenumber which means that the *ka* values relates to the wavelength λ and the Chu-radius a as:

$$ka = \frac{2\pi}{\lambda}a \tag{6.3}$$

6.1.2 Bandwidth Limitations

At first glance the drawbacks of decreased bandwidth as an effect of decreasing the antenna size may seem miniscule but in reality several effects will start to emerge that will severely limit the antennas performance. The most obvious drawback is if the bandwidth of the antenna starts to decrease to below that of the allocated frequency band used for transmission thus limiting the number of channels that can be used, and in the extreme case, not supporting the using of even a single channel (the bandwidth of the channel is directly dependant on the symbol-rate and is not only a single frequency).

Equation (6.2) can be used to find the minimum radius a for any arbitrary antenna structure that fulfils the bandwidth requirements of the intended application. Figure. 6.1 shows the realizable area for a lossless 22MHz bandwidth Wi-Fi antenna using equation (6.2). This puts a very real and straightforward limit on how small an antenna can be expected to be. In reality, however, an antenna design very rarely manages to push the performance close to the Chu-limit.

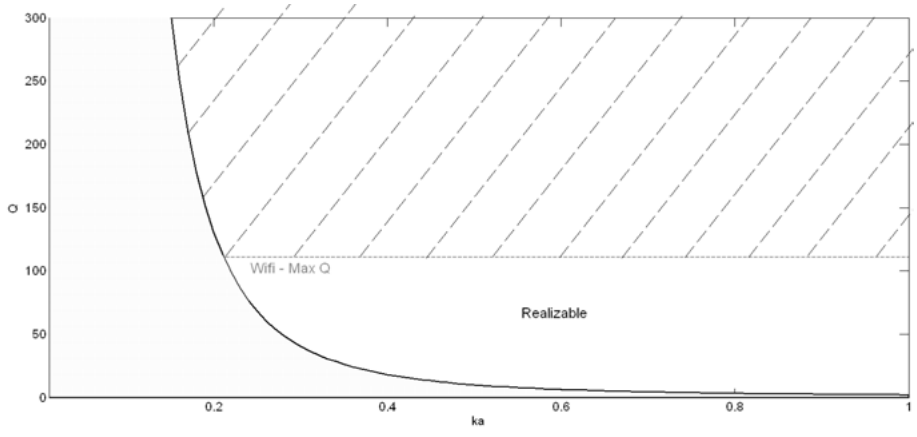

Figure 6.1. Minimum achievable Q value of antenna and upper limit set by bandwidth requirements of transceiver

Even if the bandwidth is wide enough to accommodate the desired communication channel other limiting effects also starts to take place. One effect is the sensitivity of the antenna and effect of detuning, which will make the antenna very sensitive as to how it is mounted. Another is the link between a high Q value and antenna losses, i.e. can the antenna remain highly efficient as the size decreases?

Assuming that the generator could be matched to an arbitrary low resistance load the total power consumed by the antenna can be described as

$$P_{tot} = \frac{|I|^2}{2}\left(R_{rad} + R_{loss}\right) \tag{6.4}$$

Where P_{tot} is the total power consumed by the antenna, I is the current fed to the antenna, R_{rad} is the radiation resistance and R_{loss} is loss resistance in the system. Regardless of how well engineered the antenna structure is there will *always* be losses involved. This means that regardless of how narrowband the antenna is allowed to be there will always be a point (assuming the magnitude of the radiation resistance gets continuously smaller as the antenna size decreases) where the energy consumed by the radiating charges will get smaller than the energy lost in other parts of the antenna.

Figure 6.2. illustrates the issue of finite conductivity vs size for an electrically small loop antenna operating at 433 MHz. In this example the loss resistance due to finite conductivity equals the radiation resistance at a radius of 2 cm (corresponding to a *ka* factor of approximately 0.2). At this point the antenna has -3dB efficiency and regardless of the matching network feeding the antenna it is not possible to raise this value.

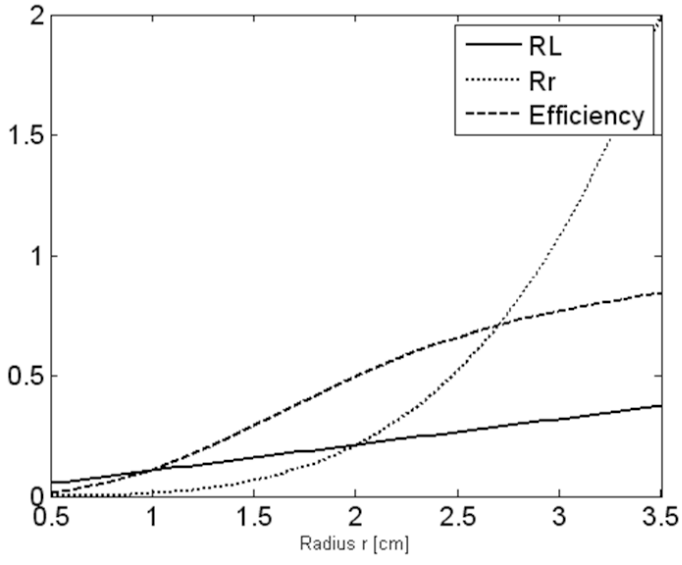

Figure 6.2. Efficiency limit of small loop antenna due to finite conductivity

In order to provide an example, the effect of loss resistance in a coil is investigated; Consider a loop antenna made of copper with a loop radius of 5 cm. The loss resistance is given by [13] as

$$R_L = \frac{a}{b}\sqrt{\frac{\omega\mu_0}{2\sigma}}N \tag{6.5}$$

Where a is the radius of the loop, b is the radius of the wire, w is the angular frequency, σ is the conductivity of copper and M is the number of turns. The radiation resistance of the same loop is given by [13] as

$$R_r = 20\pi\left(\frac{2\pi a}{\lambda}\right)^4 N^2 = 20\pi\left(\frac{a\omega}{c}\right)^4 N^2 \tag{6.6}$$

Where c is the speed of light. Consider a 433MHz loop antenna with a radius of 4 cm and a wire radius of 0.5 mm. The conductivity of copper is taken as $\sigma = 5.7\text{x}10^7$. This gives $R_L \approx 0.22$ Ohm and $R_r \approx 0.21$ Ohm. As can be seen, due to the finite conductivity of copper, the total efficiency is $\eta \approx 0.21/0.22 \approx 49\%$. As the loop gets smaller the radiation efficiency continues to decrease due to the losses in the copper. This provides a good example of the very real physical limitations that appears as the antenna decreases in size.

The reader could at this time point out that using larger wire diameters, increasing the conductivity etc. could remedy the problem. This is of course

true and when designing an electrically small antenna all these parameters would be optimized, even so, at some point the design reaches a maximum where further improvements become impossible.

6.1.3 Multiple Antennas

Wireless sensor devices are frequently set-up in indoor environments, in these kinds of setups there are usually many objects obstructing and reflecting the transmitted signals. Due to the large amount of obstructions and scattered signals numerous propagation paths exists between the transmitter and receiver which can causes large variation of signal strength depending of node placement. If the environment can be considered static the wireless device may incorporate multiple antennas in order to modify the characteristics of the received signals.

In order to have a good antenna efficiency the antenna coupling to freespace must be maximized and reflected power kept low. This can be achieved by having the correct matching between the antenna element and the generator/load. The first key-point to understand is the fact that if there is a coupling between two antennas used in the sensor platform and both elements are used at the same time a current on one element will induce a current on the other element. This will cause the input impedance of that element to change. This means that the antenna element that was once perfectly matched is no longer matched because the current induced by neighbouring antennas caused the input impedance of the matched element to change. In order to prevent this effect from severely reducing the performance of the system the change needs to be characterised and the system adjusted to take this phenomenon into account.

In order to be able to understand how the antenna interaction works the concept of mutual coupling and thus mutual impedance between elements must be understood. Figure 6.3. shows a schematic view of two antenna elements and the mutual impedance between the elements. In a system consisting of k elements the mutual impedance between two elements is

$$Z_{ij} = \left. \frac{V_i}{I_j} \right|_{I_k = 0 \; for \; k \neq j} \tag{6.7}$$

Where V_i is the voltage on element i induced by the current I_j on element j and I_k is the current on the k element. For example, Z_{12} describes how large the voltage induced on element 1 is as a function of the current driven on element 2.

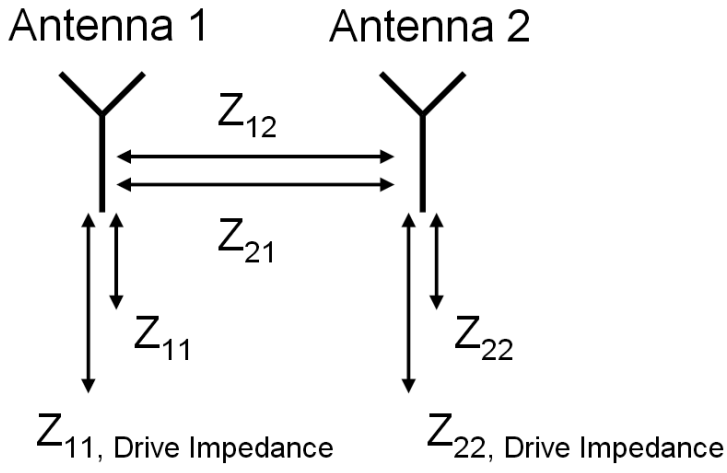

Figure 6.3. Model of two coupled antenna elements

If the mutual impedance between two elements is known the engineer can predict how a current (signal) induced on one element affect the other. The voltage induced on antenna element 1 can be described as [14]

$$V_1 = Z_{11} I_1 + Z_{12} I_2 \tag{6.8}$$

Where Z_{11} is the input impedance of the antenna with no other excitations active on neighbouring elements and Z_{12} is the mutual impedance between element 1 and 2. This allows the *antenna drive impedance* to be defined as

$$Z_{1d} = Z_{11} + Z_{12} \frac{I_2}{I_1} \tag{6.9}$$

If the amplitudes of the currents induced on both elements are assumed to be equal the behaviour of drive impedance as a function of the induced currents can be expressed as

$$Z_{1d} = Z_{11} + Z_{12} e^{j(\varphi_2 - \varphi_1)} \tag{6.10}$$

Where φ_1 and φ_2 is the phase of the induced currents. As can be seen the total drive impedance is a function of the phase difference in the feed signal to the two antenna elements. This has a couple of implications, the first one being that if the antenna system is to be used as a simple two element phased

array to give a controllable radiation pattern the matching to the antenna is going to vary as the phases varies. Using a single linear passive matching network is thus unable to prove a perfect match over all phase configurations [15]. If passive matching is used the node is going to have a drive impedance that varies as a function of the relative phase fed to the elements.

The issue with mutual coupling affecting the drive impedance of a two antenna element system can ideally be remedied by making sure the mutual impedance between the two elements are kept at a minimum. This can, however, be difficult if the total volume allocated is limited. In this case a trade-off has to be performed between the simplicity of the matching network (passive versus active matching), the variation of the reflection coefficient and the total transmitted power of the device. If the mutual impedance and the self impedance of the elements is known the drive impedance can, in most cases, be matched to provide a constant reflection coefficient over all phase angles if the magnitude of the reflection coefficient is not requires to be 0. This makes sure that the power supplied to the antennas are kept constant.

It should be noted here that even if the antennas are matched in such a way that the reflection coefficient is kept constant under all different feeding phases this does not provide a constant radiated power from the system. This can easily be seen by considering the real part of equation (6.10). The real part, assuming a lossless system, can be described as

$$R_{1d} = R_{rad} + R_{12}\cos(\varphi_2 - \varphi_1) - X_{12}\sin(\varphi_2 - \varphi_1) \tag{6.11}$$

Where R_{rad} is the radiation resistance of the antenna element. The total efficiency of antenna 1 then becomes

$$\eta_1 = \frac{R_{rad}}{R_{rad} + R_{12}\cos(\varphi_2 - \varphi_1) - X_{12}\sin(\varphi_2 - \varphi_1)} \tag{6.12}$$

As can be seen the total efficiency of element 1 will be a function of the relative phase between the two feeding currents. This means that even if the system is matched in such a way that the antenna elements always accepts the same amount of power from the generator the total radiated power is going to vary as a function of the relative phases.

7. Hemispherical Coil Antennas

In the field of antenna theory there are a few basic antenna types which are especially interesting as candidates for electrically small antennas. One such design was presented by Wheeler [4] and concerns the design of spherical coil antennas. As was discussed in previous chapters the lowest obtainable Q value of a electrically small antenna is closely linked to the effective volume which it occupies. In this sense spherical antennas are especially interesting as a sphere shape provides the highest volume for a given surface area. This means that spherical antennas gets very close to the Chu-Limit.

The biggest drawback of spherical antennas comes from the practicality of the design. A completely spherical antenna is hard to add to a reasonable design. Therefore several designs has appeared that makes use of half sphere structures mounted on a ground plane [16,17] This provides a good tradeoff between electrically small designs which can also be practically mounted. The correspondence between hemispherical antennas and spherical ones can be compared to that of dipoles vs. monopoles. However, a direct parallel may not be fully suitable as hemispherical antennas often utilizes two or more conductors rather than one single rotating conductor.

Two main methods of manufacturing hemispherical coil antennas are presented, one based on a stretchable PDMS substrate with conductor channels filled with Galinstan, a liquid metal alloy. The other method is based around printed conductors on thermoforming plastic substrates. The main advantage of both methods is the possibility to manufacture the antenna pattern on a planar surface which are then deformed to provide a spherical surface. The two antenna designs presented in this chapter covers [PAPER I] and [PAPER V].

7.1 Design Considerations

The combined advantages of hemispherical antennas makes for a very suitable antenna design for wireless sensors. One of the main issues, however, is suitable manufacturing techniques for said antenna types. The hemispherical shape makes for a much more complicated structure than the standard planar antennas typically seen in wireless sensors. Therefore a large part of the presented work focuses on novel manufacturing methods for these antenna types.

It should be noted, however, that the mandatory presence of a ground-plane for any hemispherical helix antenna carries surface currents below and around the helix structure thus making the exact limit of the radiating structures harder to define and implies that the actual Chu-radius is slightly larger than the radius of the helical coil. The difficulty of defining an exact value puts a small ambiguity in the calculated Chu limit for the antenna structure and as such it is important to point out the definition of the estimated Chu radius for the calculated theoretical minimum Q-values.

7.1.1 Inverse Spherical Projection

In order to properly pattern the planar substrate in such a way that the correct spherical structure is achieved after inflation, a planar to spherical projection must be performed to map the planar pattern to a spherical one and vice versa. The planar to spherical projection performed in the following sections are performed as described in Figure 7.1. As can be seen in the figure the coordinates of a point on the planar, un-inflated surface can be mapped to a point on the inflated hemisphere, described in Cartesian coordinates, as follows:

$$x_2 = \arcsin\left(\frac{\rho}{\left[\frac{1}{2}\left(\frac{r_0^2}{h_0}+h_0\right)\right]}\right)\frac{r_0}{\arcsin\left(\frac{r_0}{\left[\frac{1}{2}\left(\frac{r_0^2}{h_0}+h_0\right)\right]}\right)}\cos(\varphi) \tag{7.1}$$

$$y_2 = \arcsin\left(\frac{\rho}{\left[\frac{1}{2}\left(\frac{r_0^2}{h_0}+h_0\right)\right]}\right)\frac{r_0}{\arcsin\left(\frac{r_0}{\left[\frac{1}{2}\left(\frac{r_0^2}{h_0}+h_0\right)\right]}\right)}\sin(\varphi) \tag{7.2}$$

where ρ is the radial distance of the surface point, h_0 is the total height of the inflated substrate and φ is the azimuthal angle, all described in cylindrical coordinates. The variable r_0 is the radius of the ring fixture holding the substrate in place. A cylindrical coordinate system is chosen here due to the fact that an antenna structure is usually given in Cartesian coordinates and

the radial distance of a surface point is easily calculated using the x and y coordinates of such a point.

7.1.2 Helical Coil Expression

The helical coil along the hemisphere can be described in Cartesian coordinates as a function of the number of turns as follows:

$$x = \pm r_0 \cos(-2\pi N t + B)\cos\left(\frac{1}{2}\pi t\right) \tag{7.3}$$

$$y = \pm r_0 \sin(-2\pi N t + B)\cos\left(\frac{1}{2}\pi t\right) \tag{7.4}$$

$$z = r_0 \sin\left(\frac{1}{2}\pi t\right) \tag{7.5}$$

$$t = [0,1] \tag{7.6}$$

where x and y is the Cartesian components of the radial distance to a given point, z is the height of the point, N is the number of turns of the antenna, B is an arbitrary rotation of the structure and t is a continuous variable from 0 to 1. The inclusion of B is given in order to provide an easy way to rotate the structure if the analytical description is using to model the antenna in a simulation software.

The total length of each individual arm can be calculated from (37)-(40) by calculating the arc-length of the to give the following length of each individual arm:

$$L = 4r_0\sqrt{N^2 + \frac{1}{16}}E(k) \tag{7.7}$$

$$k = \frac{N}{\sqrt{N^2 + \frac{1}{16}}} \tag{7.8}$$

where $E(k)$ is the complete elliptical integral as a function of k. It is seen from simulations that the current distribution along each arm is such that the total length of each arm is slightly less than half the wavelength, $\lambda/2$. From simulations it was found that approximating the physical arm length to be $L=0.45\lambda$ gives a good fit for the resonance frequency. This gives the following expression which can be used to give an approximate resonance frequency for the helical coil

$$f_0 = \frac{c}{\lambda} = 0.45\frac{c}{L} \tag{7.9}$$

where c is the speed of light. It should be noted here that this is an approximate formula which does not take into account the detuning by, for example, the permittivity of the material upon which the antenna conductors are patterned. It does, however, correspond well with simulated parametrical sweeps.

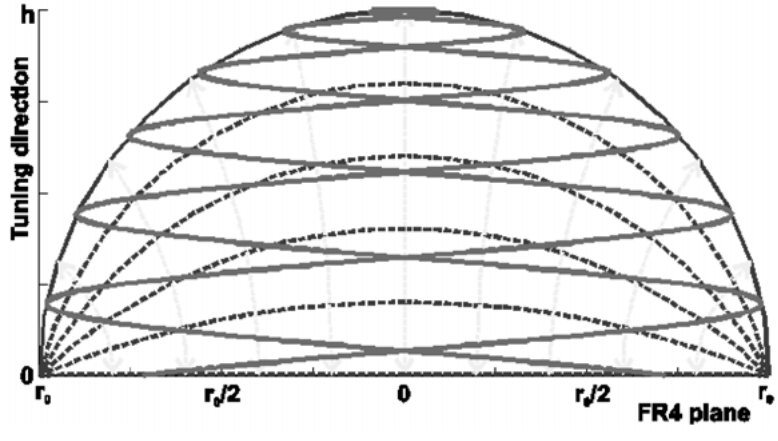

Figure 7.1. Spherical projection on plane surface

7.2 Tunable Spherical Cap Microfluidic Antenna

The first presented hemispherical antenna design is based around a stretchable PDMS substrate with channels filled with the liquid metal alloy Galinstan. The work presented describes a method of patterning planar Galinstan filled PDMS substrates which are subsequently deformed to give a hemispherical antenna structure which can be further fine tuned by controlling the inflation rate of the structure. Since the PDMS substrate is heat sensitive and direct soldering to the embedded Galinstan channels cannot be performed a coupled feed structure is proposed which provide good coupling to the antenna and removes the need for a soldered connection to the structure. The proposed coupled feed can also be used for fix structures which then do not require any direct soldering to the antenna structure.

7.2.1 Introduction

By using the manufacturing method presented Zhigang Wu et. al [18] Galinstan filled channels are patterned into the PDMS substrate to provide the antenna structure basis. The PDMS substrate provides a semi-airtight seal around the Galinstan. The wording "semi-airtight" is used to indicate the fact that a PDMS substrate does have some air-diffusion through the material, albeit at a low rate. This is important to mention as Galinstan suffers from oxidization in contact with air and further studies are recommended in order to fully characterize the aging behavior of PDMS covered Galinstan.

7.2.2 Modeling

In order to properly model the shape of the antenna structure the shape was calculated using the fact that, since the structure is that of an inflated membrane, the surface will strive to minimize the surface area of the enclosed volume. The shape achieved when the surface is inflated to a height h can be calculated using equations (7.1) and (7.2). This allows the modeling of any amount of inflation of the membrane and not only fully (perfectly spherical) inflated patterns.

7.2.3 Simulation

A parametric model of the helical structure was implemented and simulated in CST Microwave Design Studio. The resonance frequency could then be simulated as a function of the number of turns. This was used to validate the approximation expression provided in equation (7.9). The resulting data can be seen in Figure 7.2. Further simulation results are provided along with the measured data in [PAPER I].

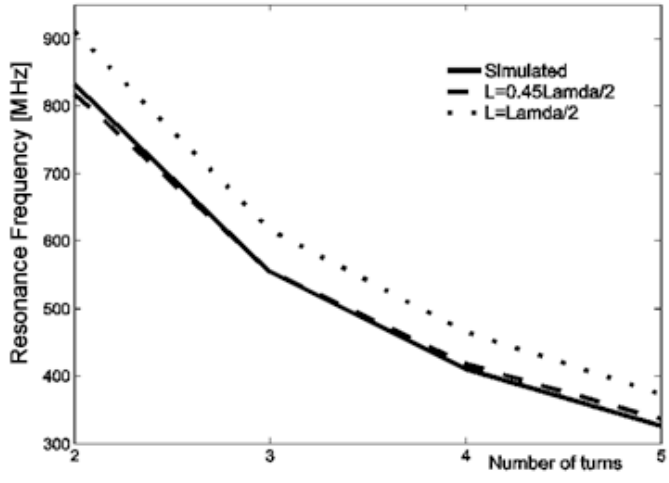

Figure 7.2. Resonance frequency as a function of the number of turns for simulated data and approximate expression

7.2.4 Manufactured Antenna

The antenna was manufactured in accordance with the process showed in Figure 7.3. A channeled PDMS substrate was prepared and filled with liquid Galinstan. The substrate was then sealed and mounted in a mounting fixture. The complete structure was then inflated using air to achieve the final structure. By adjusting the airflow the total geometry could be varied and thus also the resonance frequency of the antenna structure.

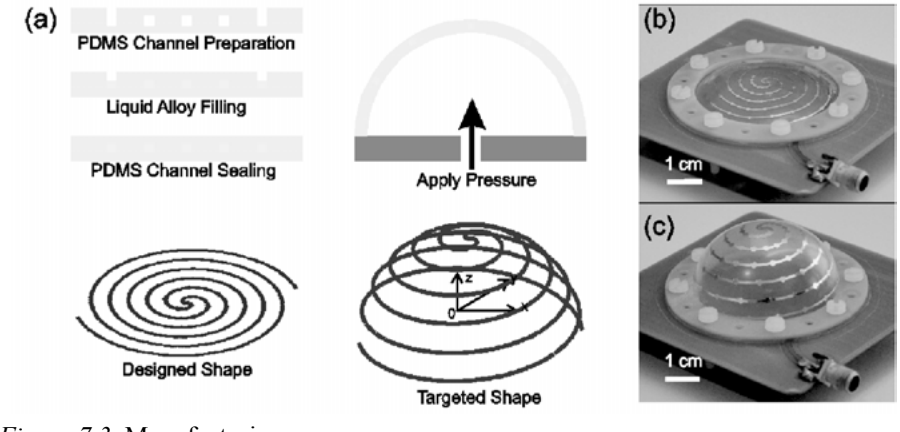

Figure 7.3. Manufacturing process

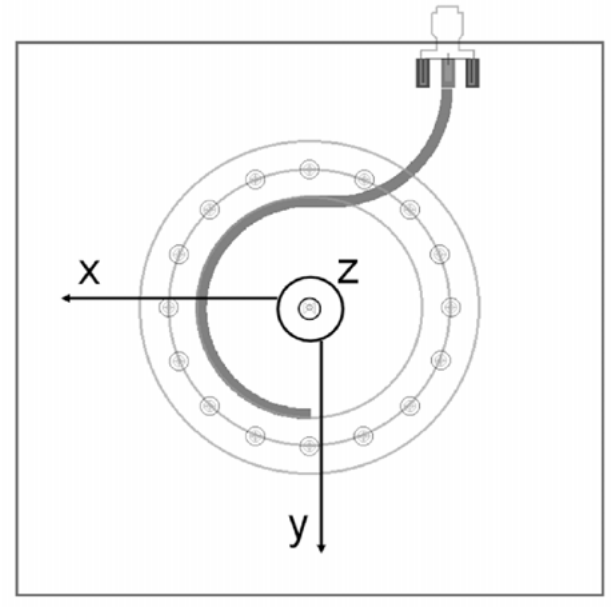

Figure 7.4. Layout of antenna holder

7.2.5 Measurements

The measured reflection coefficient for the tunable antenna is shown in Figure 7.5., while radiation characteristics are summarized in Table 1. The antenna reflection coefficient was measured using an Agilent E8364B PNA. The PNA was set to sweep from 100 MHz to 3 GHz. The silicone antenna was measured for eight different inflation heights; 5, 10, 15, 17, 20, 22, 24 and 25 mm. The resulting reflection coefficient data can be seen in Figure 7.6.

Both the theoretical Q-value based on Chu's work[8] and the measured Q-value divided by the efficiency (Q/η) were tabulated. The latter was included to validate the measured results, using the efficiency of the antenna to calculate the unloaded Q-value that should approach the Chu Limit. The tabulated values of Q/η indicate that the proposed structure, when compensated for efficiency, approaches the Chu limit for the hemispherical or nearly hemispherical cap. As was previously mentioned the proximity of the ground plane makes the exact limit of the radius of the Chu sphere difficult to define and introduces a small ambiguity in the calculated values but based on simulation results of the ground current the radius of the hemispherical structure was estimated to be 22 mm.

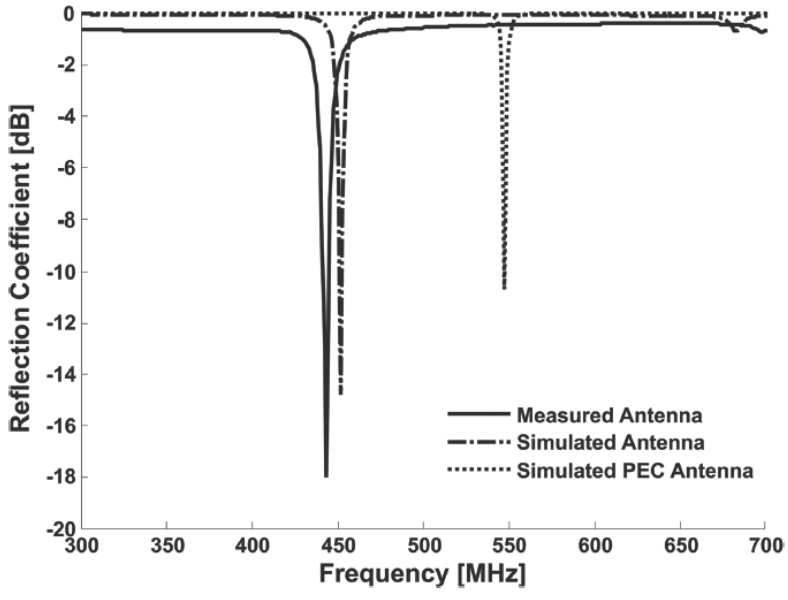

Figure 7.5. Simulated and measured reflection coefficient of the antenna when it is tuned as to a perfect spherical shape.

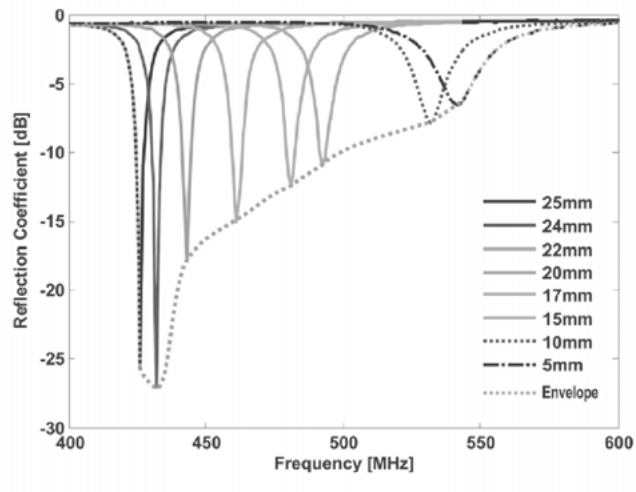

Figure 7.6. Measured reflection coefficients at different tuning states (heights).

The radiation pattern of the measured microfluidic antenna can be seen in Figure 7.7. together with the simulated radiation pattern. The measured radiation pattern shows good correspondence with the simulated one, further analysis of the measurement results can be found in [PAPER I].

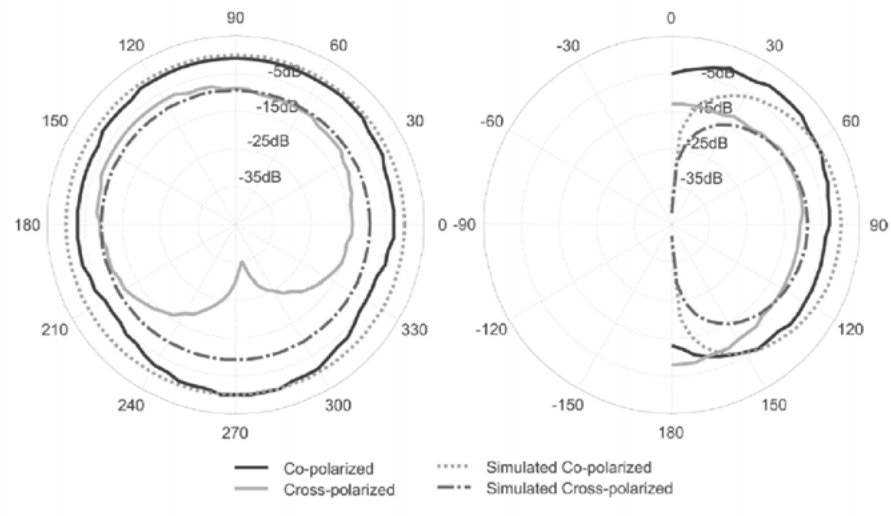

Figure 7.7. Simulated and measured radiation pattern of the antenna when it is tuned as a half sphere.

The Wheeler Cap method was used to measure the antenna efficiency. The antenna height was measured by using dielectric spacer of predefined sizes. The antenna height was measured before and after the efficiency measurements since the Wheeler Cap made simultaneous height measurements impossible. Several measurements were made to verify repeatability. As can be seen in Table 1 the maximum measured efficiency was for an inflation height of 24 mm which corresponds to a slightly overinflated structure. The main reason for obtaining the highest efficiency for this inflation relates to the fact that a larger antenna structure will experience a higher radiation resistance in comparison with the radiated power. At an inflation of 24 mm the largest radiating structure is obtained and as such the corresponding efficiency is also maximized.

Table 1. Radiation characteristics of the antenna at different tuning states.

Height [mm]	Freq. [MHz]	S11 [dB]	BW [MHz]	Corr. [dB]	FBW [MHz]	Q	η - Meas.	ka	$Q_{Chu,\ est}$	Q/η
25	426	-25.6	8	-0.7	1.9%	53	55%	0.22	95	96
24	432	-27	8	-0.7	1.9%	53	52%	0.22	102	102
22	443	-18	9	-0.65	2%	50	35%	0.20	123	143
20	461	-15.1	11	-0.6	2.4%	42	29%	0.21	109	145
17	481	-12.5	11	-0.6	2.3%	44	27%	0.22	96	163
15	493	-11	11	-0.6	2.8%	35	17%	0.23	90	206
10	532	-7.8	14	-0.55	3.6%	28	5%	0.25	72	560
5	542	-6.5	19	-0.4	5%	20	2%	0.25	68	1000

7.3 Fixed hemispherical antenna

The coil antenna presented in section 7.1 exhibits good performance with some special characteristics. For low cost sensor nodes, however, the presented design might not be perfectly suitable. Therefore a second iteration of the design based on fixed thermoformed plastic was performed. The goal of the design was to present a low cost design with a manufacturing method which could be suitable for mass production. The complete design is presented in [PAPER V].

7.3.1 Introduction

In order to adhere to the low cost requirement for antenna designs suitable for wireless sensors the antenna was constructed in such a way that it could, similar to the antenna design in section 7.1, be constructed mainly as a planar piece which is then deformed in the final production steps to achieve the hemispherical shape required. This was achieved by manufacturing the antenna out of a thermoplastic material with the antenna elements patterned using conductive ink. Figure 7.8. shows the manufactured antenna with the corresponding manufacturing process.

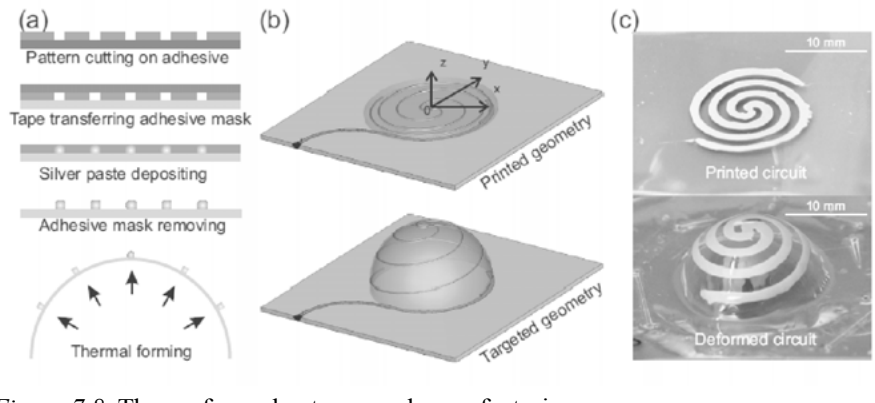

Figure 7.8. Thermoformed antenna and manufacturing process

The basic antenna parameters were decided by using equation (7.9). Although equation (7.9) should only be considered to give a rough estimate of the resonance frequency due to the inclusion of several unknowns (the precise conductivity of the conductive ink, small antenna conductor deformations induced during the thermoforming process etc.) it was considered good enough to provide initial antenna dimnsions. As can be seen in the manufactured antenna this equation gave a good estimate on the required antenna dimensions.

7.3.3 Measurements & Results

The antenna efficiency was measured in an in-house reverberation chamber connected to an Agilent E8364B PNA. Two broadband high efficiency PICA antennas was used as reference antennas. The antenna had a resonance frequency of 2.467 GHz and an efficiency of 40%.

The antenna radiation pattern was measured in a full-sized anechoic chamber and the resulting measured and simulated data can be seen in Figure 7.9. The data correspond well with the one acquired for the antenna designed in 7.1. Considering the low cost, lower quality materials used for manufacturing the authors were satisfied with the acquired performance.

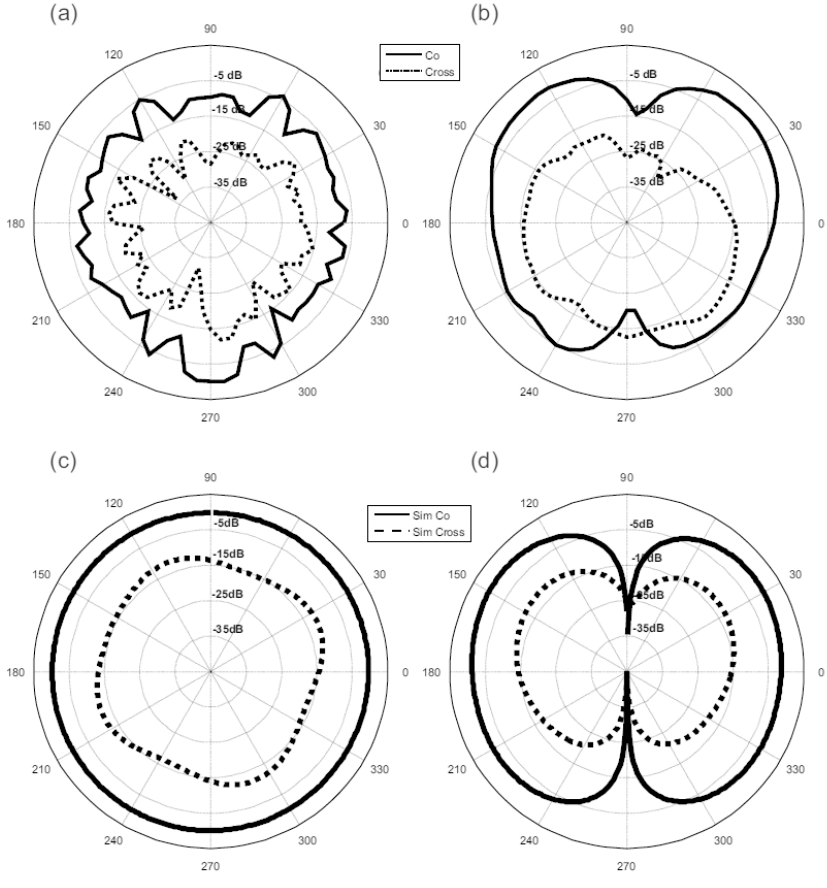

Figure 7.9. Measured and simulated radiation pattern for the proposed antenna. a) measured H-plane, b) measured E-plane, c) simulated H-plane, d) simulated E-plane

8. Conformal Dual Patch Antennas

This section describes the work performed in developing a conformal dual patch antenna for wireless sensor devices. It is intended to provide an antenna solution that improves the node performance in multiscattering environments. The proposed antenna could be considered an extreme form of conformal patch antenna where the patch conforms to the underlying structure using sharp edge-transitions. As the size of the proposed antenna structure is still in order of a quarter of a wavelength both good efficiency and reasonable bandwidth is can be expected. The antenna was embedded in the sensor housing in order to provide as large antenna volume as possible. The discussion in the following sections covers [PAPER VII] and [PAPER VIII].

8.1 Background

Including multiple antennas in an electrically small volume is a challenging task with a number of tradeoffs included. In order to provide a solution that provides a dual antenna system designed for a small wireless node a node design including two conformal patch antennas is presented. The requirement for the conformal antennas in this case was a shape that permitted the placement of the antennas on the surface electronic housing.

Previous publications exist on a number of cuboid style antennas [19, 20]. However, none of the previous antennas was deemed suitable when adding the constraint of embedding the electronics inside the housing. The main motivation for this was the fact that many of the previous cuboid antennas assume a hollow interior. Although these antennas themselves exhibit excellent performance the inclusion of hardware inside the structure can be expected to deteriorate or change the performance of the proposed structures.

8.2 Prototype Design

Work was carried out to design a dual element antenna based on two criteria; 1) The elements should provide good efficiency of an acceptable bandwidth and 2) the elements should exhibit low mutual impedance. The proposed design was drafted while considering how to include dual antennas for the node circuit-board presented in section 3. In order to reduce noise the enclo-

sure was decided to be shielded which meant that the antennas needed to be placed outside the main board. A antenna design based on conformal patches were chosen because of the advantage of having the antennas placed conformably on the board housing/shielding and the low coupling to underlying structures. Simple meandered monopole designs were considered but these experiences a substantial coupling to underlying materials whiles the groundplane of the patch antennas help shield the antenna structures from detuning due to these sources. The patches were placed along the diagonal of the casing in order to have the lower edges of the patches orthogonal in an attempt to reduce the mutual coupling.

The final proposed design shown in an exploded view can be seen in Figure 8.1. The dual patches are integrated on a metal housing, in this case made out of aluminium with both PCB and power-source (coin-cell battery) embedded within the housing. Two minor slots are integrated at the edge of the enclosure providing a connection between the RF-front end and the dual antennas. Fully sealed and coated this provides a shielded and rugged enclosure able to withstand harsh environments.

The initial prototype was designed in both ProEngineer (rereleased as Creo Parametric in 2011) and CST Microwave Studio. The ProEngineer model was used in manufacturing of the antenna structure and CST Microwave Studio was used for EM-simulations of the proposed structure. Further information about simulation results can be found in [PAPER VII] and [7].

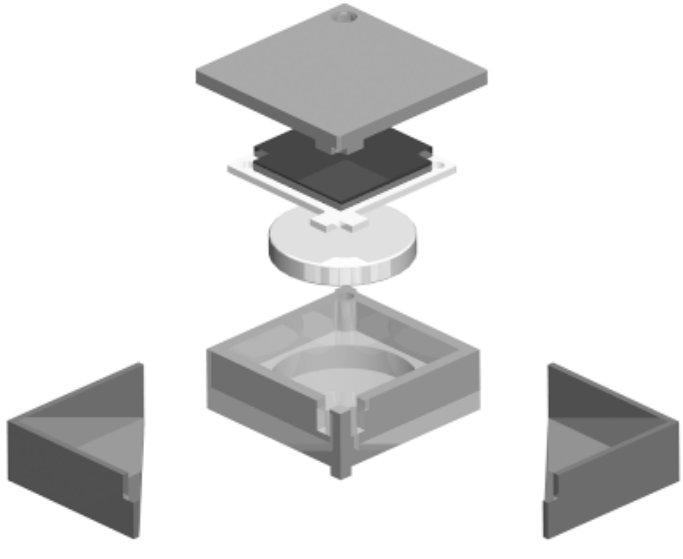

Figure 8.1. CAD model of sensornode with conformal antenna embedded in the node housing

The prototype designed was constructed using 10 mm aluminum base material and milled out using a small 3-axial milling machine. Further details concerning the manufacturing process can be found in the referred licentiate thesis [7]. Figure 8.2. shows the manufactured test antenna.

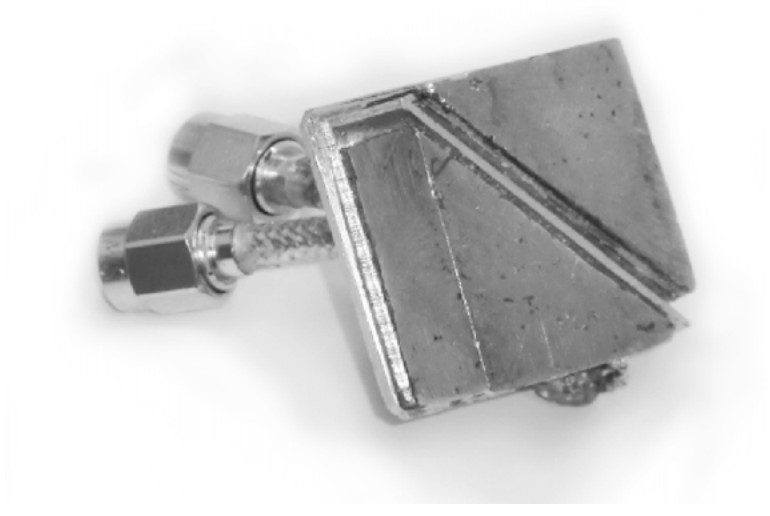

Figure 8.2. Picture of initial prototype antenna

8.3 Measurements

The manufactured antenna structure were measured and evaluated for a number of applications. Two different versions of the proposed antenna were evaluated, one operating at 3.55 GHz and one at 2.45 GHz. Provided below is some of the key performance figures for the antenna design

Using the manufactured antenna prototype S-parameter and efficiency measurements were carried out using an Agilent E8364B PNA. A full S-parameter sweep was made from 0.1 to 6GHz and can be seen in Figure 8.3. The presented data is for the first 3.55 GHz prototype. As can be seen the antenna is operated in the second resonance mode. The reason for this was that the second resonance mode provided a much more favorable radiation pattern when considering the antenna design as a two element steerable array.

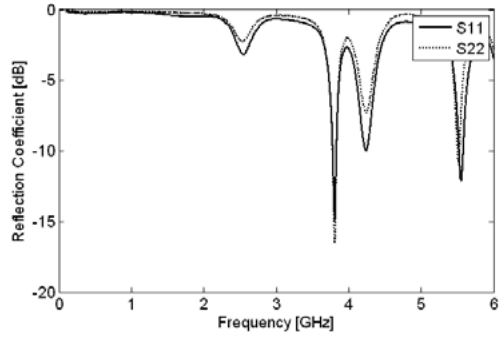

Figure 8.3. Measured reflection coefficient of initial prototype antenna

The antenna efficiency was measured using a reverberation chamber. The chamber used two broadband PICA-antennas as reference antennas. During reference measurements and antenna measurements both reference antennas and DUT was present inside the chamber and all antenna connections connected to 50 Ohm loads. The sweep duration was set to 20 seconds with two independent mode stirrers. The measured radiation efficiency can be seen in Table 2.

Table 2. *Efficiency Measurements*

Resonance Mode	FREQUENCY	Radiation Efficiency
First	2.54GHz	-4.1dB
Second	3.81GHz	-4.3dB
Third	4.27GHz	-7.9dB

When used as a two element phased array the antenna radiation pattern can be modified greatly dependant on the relative phase shift between the two antenna feeds. The simulated radiation pattern can be seen in Figures 8.4. and 8.5. The simulated antenna patterns are included below as they provide the clearest picture of the antenna radiation patterns, additional simulated and measured radiation patterns can be found in [PAPER VII]. By adjusting the relative phase between the elements in steps of of 0^o, 90^o, 180^o and 270^o degrees the radiation pattern can be controlled in four distinct steps. This allows the antenna to increase the probability of obtaining a good signal-strength between transmitter and receiver in a multiscattering environment.

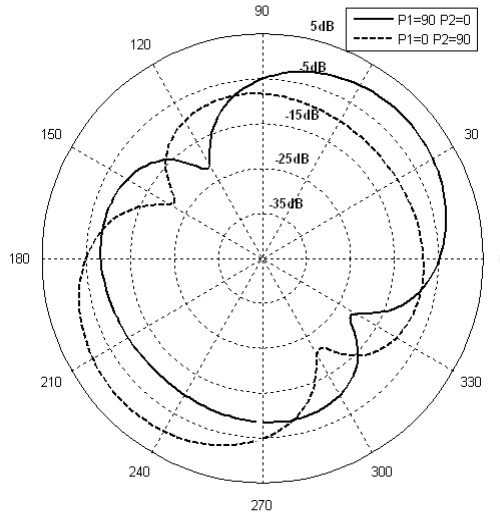

Figure 8.4. Simulated radiation pattern for dual fed antenna elements along the x-y plane

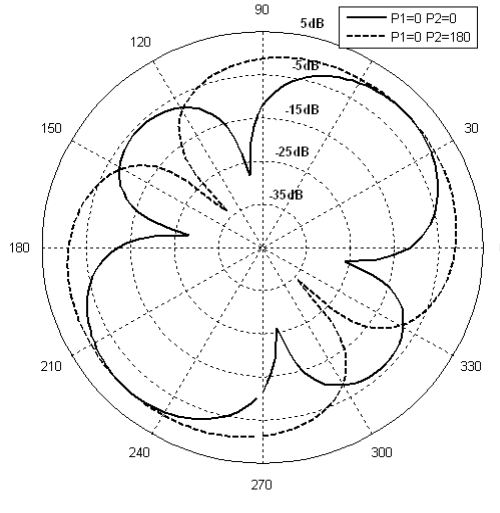

Figure 8.5. Simulated radiation pattern for dual fed antenna elements along the x-y plane

Since the antenna comprises of two fed antenna elements the change in relative phase between the feed signals will cause a change in drive impedance as explained in section 6. Figure 8.6. show the measured drive impedance of a antenna element as the drive signal on the other patch is phase swept 360 degrees relative to the elements input signal.

It is important to note here that in the figure given there is no definition of the phase of secondary signal. This is simply due to the fact that there was no way, in the setup used, to phase-lock the network analyzer signal used to feed the primary element with the signal generator feeding the second source. As such the figure only gives the total span of drive impedance seen.

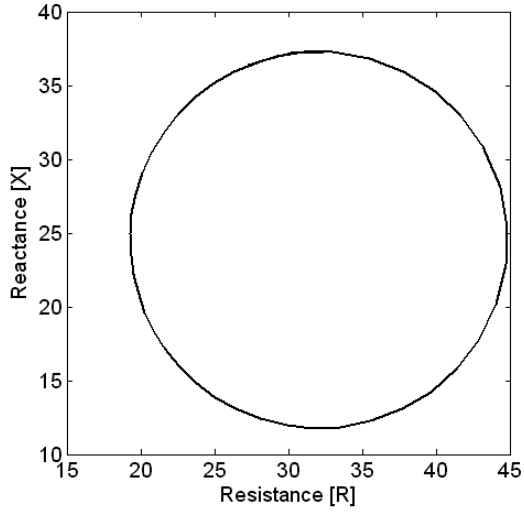

Figure 8.6. Measured drive impedance of the primary element as the input signal of the second element is swept between 0 and 360 degrees.

8.4 Performance Gain Evaluation

The performance gain of the proposed antenna structure was measured in an office environment by placing the AUT at a fixed location and connected to a signal generator. The antenna used was designed for 4 different antenna configurations achieved by varying the phase of the two antenna feeds. The differential phase shifts evaluated was 0^o, 90^o, 180^o and 270^o. The topology and measured locations can be seen in Figure 8.7.

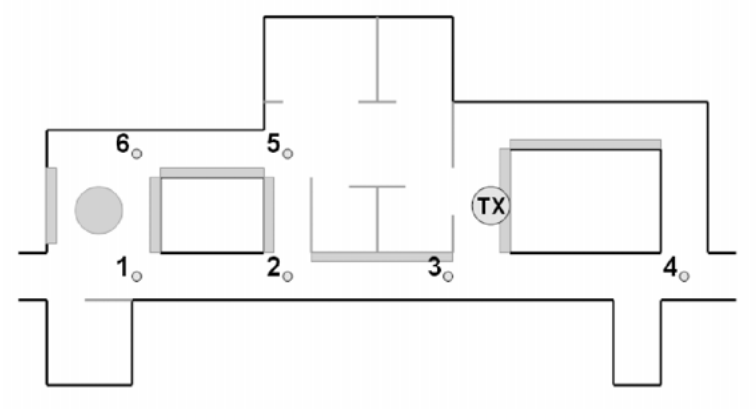

Figure 8.7. Topology of environment used for antenna performance gain evaluation

The amplitude of the received signal in these points was measured for each of the four individual antenna configurations. For the receiver antenna a vertically placed PICA antenna connected to a spectrum analyzer was used. The initial locations of the nodes were distributed over the environment to give a default unknown pathloss between transmitter and receiver.

The measured data can be seen in Table 3. The data in the table was normalized to the single highest received signal in order to make the performance of the antenna easy to read. As can be seen from Table 3 no single antenna configuration was found to be consistently superior corresponds well with the expected advantage of using a system based on multiple antennas in a multi-scattering environment. A maximum gain of 19 dB was recorded for location 2. The minimum gain recorded was 4 dB at location 3. This was most likely due to the close distance to the transmitter giving a strong line-of-sight component.

Table 3. *Measured Data*

Location	Normalized Signal Strength			
	0^o	90^o	180^o	270^o
1	-16dB	-27dB	-17dB	-12dB
2	-11dB	-13dB	-8dB	-27dB
3	-1dB	-5dB	0dB	-5dB
4	-13dB	-12dB	-17dB	-16dB
5	-7dB	-8dB	-22dB	-6dB
6	-21dB	-15dB	-27dB	-17dB

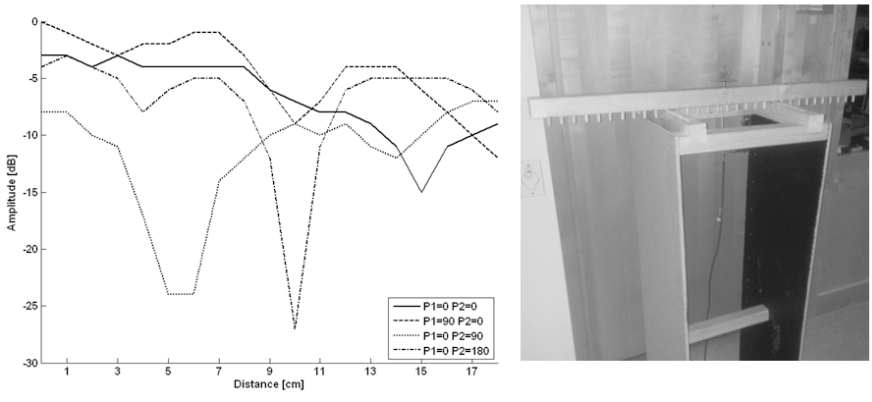

Figure 8.8. Measured received signal strength along a linear spatial sweep measured at location 6 along with measurement setup

In order to further validate the multiscattering behavior of the environment and the performance gain of the proposed antenna several linear spatial sweeps were made. The receiving vertical PICA antenna was moved along an 18 cm linear track and the received signal strength recorded once every centimeter. The fixture used for the measurements can be seen in Figure 8.8. The received signal strength as a function of location for each of the four phase shift combinations was measured. The resulting data can be seen in Figure 8.8. As can be seen from the collected data the environment exhibits the characteristics of a multipath environment where the signal strength varies strongly over displacements in the wavelength scale. The data show an approximate distance between fading null and nearest peak of 4 to 9 cm corresponding to 0.5 - 1 λ. The data also shows that each of the four different antenna radiation patterns experienced a different spatial fading along the measured track. This data shows that by selecting the proper setting of the antenna feeds can significantly increase the performance of the node under multiscattering conditions.

The multipath behavior of the environment the signal strength at location six was evaluated in a 3.55 x 2.84 λ grid with a resolution of 0.355 λ. The measurement setup was based on a gridded antenna holder made of dry wood with no metallic parts. The receiving antenna consisted of a PICA

antenna placed co-polarized in relation to the transmitting antenna (if no multiscattering effects would have been present). The resulting signal strength variation as a function of antenna displacement can be seen in Figure 8.9. The maximum variation was 19 dB.

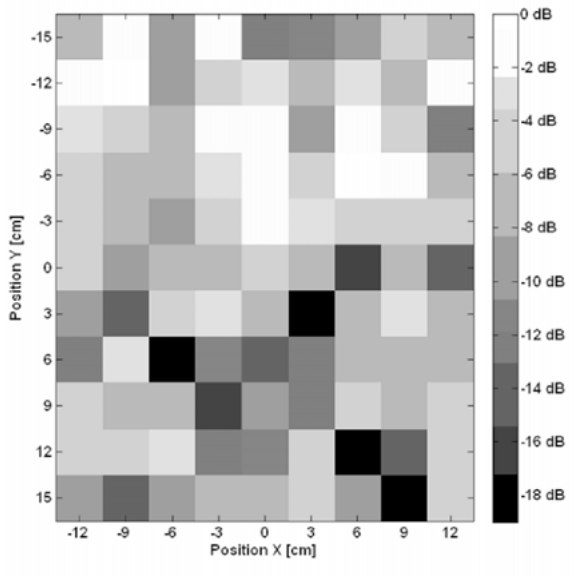

Figure 8.9. Measured normalized received signal strength as a function of antenna position

Measurements from the test environment show that the node experienced strong multiscattering effects and spatial fading. Data show a strong variation of 19 dB over a distance of only a fraction wavelength. These measurements further validates that the environment used for testing can be considered a good example of a typical multiscattering environment in which an indoor sensor-network might be deployed.

9. Summary Of Papers

9.1 Paper I: *A Tunable Spherical Cap Microfluidic Electrically Small Antenna*

Magnus Jobs, Klas Hjort, Anders Rydberg, Zhigang Wu

The paper presents the design of a hemispherical antenna made out of a stretchable substrate (PDMS) with antenna conductors made out of liquid metal (Galinstan). The choice of material gives the antenna the ability to deform without damaging the structure. After presenting the antenna design which also provides a analytical expression for estimating the operating frequency of the antenna as well as a coupled, solder-less, antenna feed, the paper goes on to show how the operating frequency can be adjusted by inflating and deflating the antenna structure.

The main purpose and contribution of the paper is to provide a stretchable antenna design and corresponding manufacturing process as well as a solderless feed which removes the risk of heat damage to the antenna structure materials. Also, the expression for operating frequency provided gives a good rule of thumb for estimating the operating frequency of said structures. The overall design provide a electrically small antenna which still maintains a good efficiency in relation to the size. The proposed design is also suitable to the placed on conducting surfaces. The presented antenna operates in the 433 MHz band and beyond.

9.2 Paper II: *Antenna Diversity With Opportunistic Combining for ASK Systems With Single Channel Receivers*

Magnus Jobs, Mathias Grudén, Paul Hallbjörner, Anders Rydberg

The paper proposes a way to use discrete phase sweep transmit diversity (DPSTD) to improve node performance. A prototype circuit is designed and used to make test measurements in a fading indoor environment. The measured results are used to calculate the potential diversity gain of the device. Although previous paper on analog phase sweep transmit diversity has been

found it is, to the authors knowledge, first time a discrete form is used in order to provide a diversity scheme suitable for wireless nodes. The authors also acknowledge that the most crucial parameters which needs to be considered before the circuit is implemented in an application is the potential spectrum broadening effect of the diversity scheme.

9.3 Paper III: *Empirical Tests of Wireless Sensor Network in Jet Engine Including Characterization of Radio Wave Propagation and Fading*

Mathias Grudén, Magnus Jobs, Anders Rydberg

The paper presents the obtained performance from a wireless sensor system designed and mounted inside a running military grade jet turbine. End results show that the designed system is able to run continuously in the engine and gather temperature data during runtime. Channel performance measurements on the jet turbine is also presented which aims to guide this and further designs in how to adapted the wireless channel to cope with the fast fading environment inside the turbine.

9.4 Paper IV: *Modeling of EM Propagation in Simplified Jet Turbine Structure using Helical Rays*

Magnus Jobs, Mathias Gruden, Anders Rydberg

The paper is related to the wireless sensor network design performed for the jet turbine network. In this paper a simplified analytical model is used in order to provide further understanding of the propagation behavior inside the turbine. Using a simplified geometry a test-setup is constructed and measured data is compared to data obtained from an analytical model processed in Matlab.

The model base hypothesis is that the measured environment can be considered as a superposition of helical propagating rays which superimpose to create a average power distribution inside the structure. Good correspondence between measured and simulated data indicates that the model may be a valid assumption and shows that for the purpose of simulating the simplified geometry does a adequate job.

9.5 Paper V: *Hemispherical Coil Electrically Small Antenna Made by Stretchable Conductors Printing and Plastic Thermoforming*

Zhigang Wu, Magnus Jobs, Klas Hjort, Anders Rydberg

The paper is a continuation of the work presented in [PAPER I]. In this paper an alternative design based on thermoformed plastic with a printed conductor is presented. The same hemispherical coil antenna designed as was used in [PAPER I] is used and the estimation formula provided gives good correspondence with the manufactured antenna, which further validates the validness of the expression.

The main contribution of the paper is to provide a low cost manufacturing method for constructing electrically small, good performance hemispherical coil antennas useable in the ISM bands. The presented antenna is operating in the 2.4 ISM band.

9.6 Paper VI: *Measurements and Simulations of Wave Propagation for Wireless Sensor Networks in Jet Engine Turbines*

Mathias Grudén, Magnus Jobs and Anders Rydberg

The paper centers around wave propagation measurements inside both a full scale RM12 jet turbine as well as a half scale jet turbine. The measured data shows that the environment inside the turbine is a fast fading environment which operates as a function of the position of the turbine blades. As such it is also a highly predictive environment and low rotation speed measurements are used to predict the corresponding fading intervals expected at full engine speed rotation.

9.7 Paper VII: *Conformal dual patch antenna for diversity based sensor nodes*

Magnus Jobs, Anders Rydberg

The paper describes a dual patch antenna design to fit the package of a custom in-house wireless sensor. The antenna is designed to provide low antenna element correlation which makes it usable as a diversity enabling antenna structure for wireless nodes. The antenna is built around a solid alumi-

num housing and conformably fitted to the surface of the housing. The antenna is designed to allow the device to modify the radiation pattern by controlling the individual phase on the antenna elements. One envisioned application is the combination of the proposed antenna structure and the diversity combiner presented in [PAPER II].

9.8 Paper VIII: *Performance Evaluation of Conformal Dual Patch Antenna In Indoor Environment*

Magnus Jobs, Mathias Grudén, Anders Rydberg

This paper provides further evaluation of the potential gain of the dual patch antenna presented in [PAPER VII]. Using a typical indoor environment a cross sectional area is measured to provide data on the fading distribution in the environment and then goes on to measure the variance in gain as a function of for different antenna configurations. The antenna configurations are obtained by phase shifting the individual signals to the antenna elements and thus creating four distinctive radiation patterns.

9.9 Paper IX: *Diversity Techniques for Robustness and Power Awareness in Wireless Sensor Systems for Railroad Transport Applications*

Mathias Grudén, Magnus Jobs

This book chapter was written as a part of a book on sustainable wireless networks. The chapter provides some general oversight of diversity schemes useful for wireless sensor networks.

9.10 Paper X: *Wireless Body Area Network (WBAN) Monitoring Application System(MASS) for Personal Monitoring*

Magnus Jobs, J. Bestoon, F. Lantz, B. Lewin, E. Jansson, J Antoni, K. Brunberg, P. Hallbjörner, A. Rydberg

The paper describes a developed wireless body area network (WBAN) used for monitoring of human test subjects. The proposed system was developed within the WISENET project and provides accelerometer data and location

data (GPS) which are uploaded via a GPRS link and enables the server to calculate the limb positioning the test subject.

10. Summary in Swedish

Arbetet som presenteras i denna avhandling fokuserar i huvudsak på design och utveckling av trådlösa sensornät för både kroppsburna tillämpningar samt sensornät monterade i krävande miljöer. Trådlösa sensornät är nätverk bestående av små elektroniska enheter med förmågan att kommunicera trådlöst mellan olika enheter (noder). På så sätt kan det kompletta systemet samla och vidarebefodra data för att ge en komplett bild av hur det övervakade systemet beter sig. Materialet i denna avhandling fokuserar på två olika nivåer, kompletta trådlösa system som tagits fram för specifika uppgifter samt deltekniker som kan användas för att öka prestandan på trådlösa noder generellt.

I den första delen av avhandlingen behandlas två kompletta trådlösa system. Det första systemet har som tagits fram under ett samarbete mellan Uppsala Universitet, Hectronic AB och Totalförsvarets forskningsinstitut inom det VINNOVA finansierade Vinn Excellence Centret WISENET. Systemet är ett kroppsburet system som ger användaren möjlighet att på avstånd följa en individs status och rörelse genom terräng utomhus.

Det andra systemet som har tagits fram är ett komplett system för statusövervakning av fläktsteget i en RM12 jet turbin där arbetet skett i ett samarbete mellan Uppsala Universitet, GKN Aerospace Engine Systems, Sweden samt ÅAC Microtec AB. RM12 motorn är den jetmotor som används i det svenska stridplanet Jas 39 Gripen. Arbetet skedde under ramarna för WISEJET projektet och utmynnade i ett komplett system som under testdrift kunde mäta motortemperaturen i fläktsteget på en RM12 motor. Arbetet inkluderade en avsevärd mängd mätningar och tester för att verifiera att prestandan hos noderna fortfarande var god efter en skarp installation i jetmotorn.

Den andra delen av avhandlingen behandlar nya delsystem som kan användas för att förbättra prestandan hos trådlösa sensornät. Dessa inkluderar elektriskt små antenner anpassade för de storlekskrav som finns på trådlösa noder, alternativa former av diversitet för inbyggnad i trådlösa noder samt utveckling av nya trådlösa noder för test och utveckling. De antenndesigner som presenteras inkluderar två former av elektriskt små halvsfäriska spolantenner. Ett av huvudmålen med dessa antenner är att kunna ta fram dem genom en enkel tillverkningsprocess med låg produktionskostnad medan prestandan på antenner bibehålls hög. En design och metod för tillverkning av antenner i strechbara silikonbaserade material presenteras

tillsammans med en tillverkningsmetod baserad på värmeformade plastsubstrat med tryckt silverbläck som ledare.

En annan form av antenndesign som presenteras är en konform patchantenn med två element som placerats på skalet till en packeterad sensornod. Huvudpoängen med den presenterade designen är att ge ett exempel på hur flera antenner kan placeras på en elektriskt liten sensor och ge möjlighet att förbättre prestandan hos noden då den arbetar i fädande miljöer.

Acknowledgements

In the end of all things all we have to do is to be thankful for all the people helping and inspiring us to get to where we are. With this said I would like to give special acknowledgements to the following:

First and foremost I would like to give my deepest gratitude for all my family and friends back in my hometown Leksand. All who tolerated (and survived?) all the crazy projects and adventures which set my on my path to Uppsala. To my father Mikael Jobs and his wife Johanna Jobs, my grandfather and grandmother Pär Jobs and Rut Jobs. For my brothers and sister Martin, Niklas and Evenlina Jobs. For all my close aunts and cousins and for my childhood friends Andreas Mats, Mikael Johansson, Patrik Daniels, Joel Nises, Markus Erson Bonde, Henning Lundin as well as all other close friends.

Also a big acknowledgement goes out to Ingrid Almkvist for all putting up with me all these years whom has provided both a pillar in stormy weather as well as a wind in my sails when I needed it.

I would also like to give my deepest acknowledgements to my supervisor, Professor Anders Rydberg and my colleagues Dr. Robin Augustine, Dr. Dragos Dancila and Dr. Sujith Raman. As well as my colleagues at Solid State Electronics for all good advice and invaluable time teaching classes together with you guys.

A special acknowledgement and thank goes out to Mathias Grudén whom I worked in close cooperation with as a colleague and friend over many years.

I would also like to thank all the people and friends at the Division of Signals and Systems, Adrian Bahne, Annea Barkefors, Simon Berthilsson, Rikke Apelfröjd, Fredrik Bjurefors as well as all other excellent people in the group!

For the work carried out within Uppsala Vinn Excellence Centre for Wireless Sensor Networks, WISENET, I would like to thank VINNOVA for supporting the projects.

For all involved parties in the WISEJET project I would like to give my thanks for all the staff from GKN Aerospace Engine Systems, Sweden and the people at ÅAC Microtec AB for sharing all their deep knowledge of high performance electronics and engine design.

I would also like to give a big thank to the staff at Upwis AB lead by Kjell Brunberg, whose dedication to embedded wireless system has been a treasure chest of knowledge!

Finally a big thank you to all other people whom I've met during my time living, working and studying in Uppsala. You have all been invaluable!

Magnus Jobs
February 2015

Bibliography

1. Smart Dust: BAA97-43 Proposal Abstract, POC: Kristofer S.J. Pister
2. Gartner, Inc.,56 Top Gallant Road,Stamford, U.S.A.
3. F. Lantz, B. Levin, D. Andersson "Metoder och tekniker för beslutsstöd för övervakning av individstatus"FOI-R--3092--SE, 2010
4. H. A. Wheeler, "The Spherical Coil as an Inductor, Shield, or Antenna", Proc. IRE 1958 , 46 , 1595-1602
5. IEEE Computer Society, "802.15.1 IEEE Standard Part 15.1: Wireless medium access control (MAC) and physical layer (PHY) specifications for wireless personal area networks (WPANs)", IEEE 802.15.1™-2005
6. M. Jobs “Wireless Body Area Network – Monitoring Application System”, Uppsala University, Master Thesis, 2009
7. M. Jobs "Design and Performance of Diversity based Wireless Interfaces for Sensor Network Nodes" Licentitate Thesis, Uppsala University, 2013, urn:nbn:se:uu:diva-198734
8. L. J. Chu , "Physical Limitations Of Omnidirectional Antennas" , Technical Report NO. 64, may 1, 1948, MIT
9. R. F. Harrington, “Effect of Antenna Size on Gain, Bandwidth, and Efficiency”, Journal of Research of the National Bureau of Standards- D. Radio Propagation, Vol. 64, No.1, January- February 1960
10. R. C. Hansen, "Fundamental limitations in Antennas", Proceedings of the IEEE Vol. 69, Issue: 2, 1981
11. J. S. McLean, "A Re-Examination of the Fundamental Limits on the Radiation Q of Electrically Small Antennas", IEEE
12. H. A. Wheeler, “Fundamental Limitations of Small Antennas”, Proceedings of the IRE, Dec. 1947
13. C. A. Balanis “Antenna Theory – Analysis And Design” Third Edition, ISBN: 0-471-66782-X, 2005
14. M. F. Iskander “Electromagnetic Fields & Waves” ISBN: 0132494426, 1992
15. D. Varon, G. I. Zysman "Some Properties and Limitations of Electronically Steerable Phased Array Antennas" Antennas and Propagation Society International Symposium, Vol. 5, pp. 264 - 270, 1967
16. S. R. Best "The performance properties of an electrically small folded spherical helix antenna", in Proc. of the IEEE Antennas and Propagation Society International Symposium, 2002 p. 18.
17. J. J. Adams, et. al. "Conformal Printing of Electrically Small Antennas on Three-Dimensional Surfaces" Adv. Mater. 2011 , 23 , 1335-1340
18. Zhigang ref PDMS manu method
19. I.T. Nassar, T.M. Weller, "Development of Novel 3-D Cube Antennas for Compact Wireless Sensor Nodes", Antennas and Propagation, IEEE Transactions on, Vol. 60, pp. 1059-1065, 2012
20. B.N. Getu, J.B. Andersen, "The MIMO cube - a compact MIMO antenna", Wireless Communications, IEEE Transactions on, Vol. 4, pp. 1136-1141, 2005

Acta Universitatis Upsaliensis

Digital Comprehensive Summaries of Uppsala Dissertations from the Faculty of Science and Technology 1216

Editor: The Dean of the Faculty of Science and Technology

A doctoral dissertation from the Faculty of Science and Technology, Uppsala University, is usually a summary of a number of papers. A few copies of the complete dissertation are kept at major Swedish research libraries, while the summary alone is distributed internationally through the series Digital Comprehensive Summaries of Uppsala Dissertations from the Faculty of Science and Technology. (Prior to January, 2005, the series was published under the title "Comprehensive Summaries of Uppsala Dissertations from the Faculty of Science and Technology".)

Distribution: publications.uu.se
urn:nbn:se:uu:diva-239400

ACTA
UNIVERSITATIS
UPSALIENSIS
UPPSALA
2015